The surface aerosol optical properties in urban areas of Nanjing, west Yangtze River Delta of China

B. L. Zhuang[1, *], T. J. Wang[1, **], J. Liu[1, 2], S. Li[1], M. Xie[1], Y. Han[1], P. L. Chen[1], Q. D. Hu[1], X.-Q. Yang[1], C. B. Fu[1], J. L. Zhu[3]

[1] School of Atmospheric Sciences, CMA-NJU Joint Laboratory for Climate Prediction Studies, Jiangsu Collaborative Innovation Center for Climate Change, Nanjing University, Nanjing 210023, China

[2] Department of Geography and Planning, University of Toronto, Toronto, M5S 3G3, Canada

[3] Department of Climate and Space Sciences and Engineering, University of Michigan, Ann Arbor, Michigan, USA

[*] Corresponding author, E-mail: blzhuang@nju.edu.cn; Tel.: +862589681156; fax: +862589683797

[* *]Corresponding author, E-mail: tjwang@nju.edu.cn; Tel.: +862589683797; fax: +862589683797

Abstract: Observational studies of aerosol optical properties are useful for reducing uncertainties in estimating aerosol radiative forcing and forecasting visibility. In this study, the observed near-surface aerosol optical properties in urban Nanjing are analyzed from Mar 2014 to Feb 2016. Results show that near-surface urban aerosols in Nanjing are mainly from local emissions and the surrounding regions. They have lower loadings but are more scattering than aerosols in most cities in China. The annual mean aerosol extinction coefficient (EC), single scattering albedo (SSA) and asymmetry parameter (ASP) at 550 nm are 381.96 Mm^{-1}, 0.9 and 0.57, respectively. The aerosol absorption coefficient (AAC) is about one order of magnitude smaller than its scattering coefficient (SC). However, the absorbing aerosol has larger Ångström exponent (AAE) value, 1.58 at 470/660 nm, about 0.2 larger than the scattering aerosols' (SAE). All the aerosol optical properties follow a near unimodal pattern, and their values are mostly concentrated around their averages, accounting for more than 60% of the total samplings. Additionally, they have substantial seasonality and diurnal variations. High levels of SC and AAC all appear in winter due to higher aerosol and trace gas emissions. AAE (ASP) is the smallest

(largest) in summer possibly because of high relative humidity (RH) which also causes considerably larger SC and smaller SAE, although intensive gas-to-particle transformation could produce a large number of finer scattering aerosols in this season. Seasonality of EC is different from the columnar aerosol optical depth. Larger AACs appear at the rush hours of the day while SC and back scattering coefficient (Bsp) only peak in the early morning. Aerosols are fresher at daytime than at nighttime, leading to their larger Ångström exponent and smaller ASP. Different temporal variations between AAC and SC cause the aerosols more absorbing (smaller SSA) in autumn, winter and around rush hours. ASP has a good quasi-LogNormal growth trend with increasing SC when RH is below 60%. The correlation between AAC and SC at the site is close but a little smaller than that in suburban Nanjing in spring. Atmospheric visibility decreases exponentially with increasing EC or SC, more sharply in spring and summer, and it could be further deteriorated with increasing SSA and ASP.

1 Introduction

Atmospheric aerosols have substantial influences on human health, air quality and climate changes and their loadings have significantly increased since the preindustrial times (Qin et al., 2001; Forster et al., 2007). Due to their ability of scattering/absorbing solar radiation and acting as cloud condensation nuclei, atmospheric aerosols can affect atmospheric radiation and dynamics, as well as the Earth's hydrologic cycle, leading to regional or global climate changes (Forster et al., 2007; Rosenfeld et al., 2008; Qian et al., 2009; Li et al., 2011; Wang et al., 2014; Guo et al., 2016a). Light scattering aerosols have contributed to offsetting the warming effect of CO_2 (Kiehl and Briegleb 1993) while light absorbing aerosols such as black carbon (BC) could further enhance the global warming (Jacobson 2002), especially in the high aerosol regions. Due to the warming effect of BC, the atmosphere would

become more unstable, which might result in the changes in the trend of precipitation in China over the past decades as suggested by Menon et al. (2002). Furthermore, atmospheric aerosols can be a major component in haze pollution, altering atmospheric visibility and being harmful to human health (Chameides and Bergin, 2002).

Observations and modeling studies have been conducted on aerosol optical properties and radiative forcing, as well as its climate effects on regional and global scales in the past two decades (e.g., Penner et al., 2001; Bellouin et al., 2003; Liao and Seinfeld, 2005; Yan et al., 2008; Wu et al., 2012; Zhuang et al., 2013a; 2014a; Wang et al., 2015; Yu et al., 2016). Forster et al. (2007) summarized that large uncertainties exist in estimating the aerosol radiative forcing, especially in climate models. The bias mostly results from the uncertainties in the simulated aerosol optical properties (Holler et al., 2003), which, in turn, are related to the aerosol loadings, profiles, compositions, mixing states and the atmospheric humidity. The 5th IPCC reported that the global mean direct radiative forcing ranged from -0.85 to +0.15 W m^{-2} for total aerosols and from +0.05 to +0.8 W m^{-2} for BC (IPCC, 2013). This would further lead to much larger uncertainties in the estimations of the aerosol climate effects. In East Asia, the range of simulated BC direct radiative forcing is much larger than the global one, varying from +0.32 to +0.81 W m^2 (Zhuang et al., 2013a). The uncertainty could be substantially reduced in a model if the aerosol optical properties are based on observations or if observed properties are directly used (Forster et al., 2007).

In the last three decades, China has experienced the rapidest economic growth worldwide. This leads to high emission of anthropogenic aerosols and trace gases (e.g., Guo et al., 2009; Zhang et al., 2009; Xin et al., 2014; Che et al., 2015). The anthropogenic aerosol emissions in East Asia were estimated to exceed 1/4 of the global emissions (Streets et al., 2001), resulting in more diversified

aerosol compositions, complex species and heterogeneous spatial distributions in the region (Zhang et al., 2012), especially in megacities and urban agglomerations (e.g., Beijing-Tianjin-Hebei (BTH), Yangtze River Delta (YRD) and Pearl River Delta (PRD) regions). Uncertainties of the aerosol radiative forcing and corresponding climate effects in these regions might be much larger than those of the rest of the world (e.g.: Forster et al., 2007 and Zhuang et al.,2013b). In addition, the diurnal variability of aerosol properties has been suggested to another major factors leading to such large biases (e.g., Xu et al., 2016). Therefore, it is necessary to characterize the aerosol optical properties based on observations in China, as did many studies in recent years at urban sites and in rural areas (e.g., Bergin et al., 2001; Xu et al., 2002; 2004; Zhang et al., 2004; Yan, 2006; Xia et al., 2007; Li et al., 2007; Yan et al., 2008; Andreae et al., 2008; He et al., 2009; Wu et al., 2009; Wang et al., 2009; Li et al., 2010; Fan et al., 2010; Bai et al., 2011; Cai et al., 2011; Xiao et al., 2011; Xu et al., 2012; Wu et al., 2012; Zhuang et al., 2015; Zhang et al., 2015; Li et al., 2015a; b; Yu et al., 2016). For example, Bergin et al. (2001), He et al. (2009) and Zhuang et al. (2015) presented the surface aerosol scattering and absorption properties in urban area of North and East China and they suggested that the annual mean 532 nm-AAC in Beijing was about 56 Mm^{-1} and it was 41~44 Mm^{-1} in YRD, which were much smaller than those in central to southwest China and in PRD (Wu et al., 2009; Cao et al., 2012; Tao et al., 2014) but much larger than those in rural and desert region (Xu et al., 2002; 2004; Yan et al., 2008). In addition to surface measurements, the columnar optical properties of the aerosols were also observed (Xia et al., 2007; Zhuang et al., 2014a; Che et al., 2015). Long-term measurements of the countrywide-aerosol optical depths and Ångström exponents in China from 2002 to 2013 were introduced by Che et al. (2015). In spite of intensive observation-based studies, measurements and analysis on aerosol properties in YRD region, one of the most populous regions in China, is still rather

limited. To fill the gaps in the current observational network in China and to better understand the optical properties of urban aerosols in YRD, this study will analyze the observations of aerosol scattering (SC), back scattering (Bsp), absorption (AAC), extinction (EC) coefficients and single scattering albedo (SSA), Ångström exponent of scattering (SAE) and absorbing (AAE) aerosols, as well as aerosol asymmetry parameter (ASP) in urban area of Nanjing, a major megacity in YRD. Our ultimate goals are to provide a reference when estimating aerosol radiative forcing and climate effect as well as forecasting visibility.

In the following, the method is described in Section 2. Results and discussions are presented in Section 3, followed by conclusions in Section 4.

2 Data and Methodologies

2.1 Sampling station and instruments

The sampling station is located at the Gulou campus of Nanjing University, urban area of Nanjing (32.05^{o} N, 118.78^{o} E). It is built on the roof of a 79.3 m-tall building, around which there are no industrial pollution sources within a 30-km radius but there are several main roads with apparent traffic pollution, especially at rush hours. The layout of the site and the corresponding climatology have been described in Zhu et al. (2012).

The wavelength-dependent aerosol absorption coefficient (AAC) and concentrations of black carbon (BC) were derived from the measurements using a seven-channel Aethalomter (model AE-31, Magee Scientific, USA). The wavelength-dependent aerosol scattering coefficient (SC) and back scattering coefficient (Bsp) were measured by a three-wavelength integrating Nephelometer (Aurora 3000, Australia). To make a brief comparison between surface and column aerosols, the

wavelength-dependent columnar aerosol optical depth (AOD) was observed using a Cimel sunphotometer (CE-318). The AE-31 model measures light attenuation at seven wavelengths, including 370, 470, 520, 590, 660, 880, and 950 nm, respectively, with a desired flow rate of 5.0 L/min and a sampling interval of 5 min. Aurora 3000 measures the aerosol's light scattering, including SC and Bsp at 450, 525 and 635 nm, with a sampling interval of 1 min. CE-318 measures the AOD from 340 to 1640 nm at day times. Routine calibrations and maintenances were carried out for all these instruments during the sampling periods. R-134 was used as a span gas for Aurora 3000. The aerosol inlet is located about 1 m above the roof. Data to be analyzed in this study were measured from Mar 2014 to Feb 2016 for AE-31 and CE-318 and from Jun 2014 to Feb 2016 for Aurora 3000. Meteorological data (such as relative humidity) during the sampling period are from the National Meteorological Station of Nanjing (No. 58238).

2.2 Calculation of the aerosol optical properties

The wavelength-dependent aerosol absorption coefficient (AAC) and BC mass concentration can be calculated directly based on the measured light attenuations (ATN) through a quartz filter matrix (Petzold et al., 1997; Weingartner et al., 2003; Arnott et al., 2005; Schmid et al., 2006):

$$\sigma_{\mathrm{ATN},t}(\lambda) = \frac{(\mathrm{ATN}_t(\lambda) - \mathrm{ATN}_{t-1}(\lambda))}{\Delta t} \times \frac{A}{V} \quad (1)$$

where A (in m^2) is the area of the aerosol-laden filter spot, V is the volumetric sampling flow rate (in L/min) and Δt is the time interval (=5 min) between *t* and *t-1*. σ_{ATN} is the AAC without any correction, which is generally larger than the actual one (σ_{abs}) because of the optical interactions of the filter substrate with the deposited aerosol. Generally, there are two key factors leading to the bias: 1) multiple scattering of light at the filter fibers (multiple scattering effect), and 2) instrumental response

with increased particle loading on the filter (shadowing effect). Thus, the correction is needed and the calibration factors *C* and *R* (shown in Eq. 2) are introduced to against the scattering effect and shadowing effect, respectively:

$$\sigma_{\mathrm{abs},t}(\lambda)=\frac{\sigma_{\mathrm{ATN},t}(\lambda)}{C\times R} \tag{2}$$

Collaud Coen et al. (2010) suggested that AAC corrected from Weingartner et al. (2003) (WC2003 for short, hereinafter) and Schmid et al. (2006) (SC2006 for short, hereinafter) have good agreements with the one measured by a Multi-Angle Absorption Photometer. These two corrections are similar to each other and they use the same $R(\lambda)$:

$$R_t(\lambda)=(\frac{1}{f}-1)\times\frac{\ln(\mathrm{ATN}_t(\lambda))-\ln 10}{\ln 50-\ln 10}+1 \tag{3}$$

where R =1 when $\mathrm{ATN}\le 10$ and f =1.2. However, C value is fixed in WC2003 while is wavelength-dependent in SC2006. According to Wu et al. (2013) and Zhuang et al. (2015), C in Nanjing is 3.48 in WC2003 while it is 2.95, 3.37, 3.56, 3.79, 3.99, 4.51 and 4.64 at 370, 470, 520, 590, 660, 880, and 950 nm, respectively, in SC2006. Zhuang et al. (2015) further suggested that wavelength-dependent AACs corrected by SC2006 might be more close to the real ones than WC2003's in Nanjing, although 532 nm-AACs from these two corrections are close to each other. In addition to the direct way, AAC can also be calculated indirectly:

$$\sigma_{\mathrm{abs},t}(\lambda)=[BC]\times\gamma \tag{4}$$

where [BC] is the mass concentration of Aethalometer BC (in μg/m^3) without any correction and γ is the conversion factor determined empirically from linear regression of the Aethalometer BC concentration versus the aerosol absorption measurement (Yan et al., 2008). Zhuang et al. (2015) indicated that γ from the linear regression of the Aethalometer BC concentrations (ng/m^3) at 880 nm

against the light absorption coefficient (Mm^{-1}) at 532 nm in Nanjing is about 11.05 m^2/g. It's obviously that only 532 nm-AAC can be addressed from this way. Thus, AACs corrected from SC2006 are used in this study.

Based on wavelength-dependent AAC and SC, Ångström exponent of scattering (SAE) and absorbing (AAE) aerosols are estimated by:

$$AAE_{470/660\text{nm}} = -\log(AAC_{470nm} / AAC_{660nm}) / \log(470/660) \quad (5)$$

$$SAE_{450/635\text{nm}} = -\log(SC_{450nm} / SC_{635nm}) / \log(450/635) \quad (6)$$

For purposes of comparison, AAC at 450, 525, 532, 550 and 635 nm, SC at 532 and 550 nm as well as Bsp at 532 and 550 nm were further calculated by the given coefficients and corresponding Ångström exponents:

$$\sigma_\lambda = \sigma_{\lambda_0} \times (\frac{\lambda}{\lambda_0})^{-\alpha} \quad (7)$$

where, σ_λ is the coefficient at wave length λ, α is the corresponding Ångström exponents.

Based on wavelength-dependent SC, Bsp, AAC, aerosol asymmetry parameter (ASP), single scattering albedo (SSA) and extinction coefficient (EC) are further estimated:

$$ASP_\lambda = -7.143889\beta_\lambda^3 + 7.46443\beta_\lambda^2 - 3.9356\beta_\lambda + 0.9893 \quad (8)$$

$$SSA_\lambda = \frac{SC_\lambda}{SC_\lambda + AAC_\lambda} \quad (9)$$

$$EC_\lambda = SC_\lambda + AAC_\lambda \quad (10)$$

where, β_λ is the ratio of Bsp to SC at wavelength λ. Eq. 8 derives from Andrews et al. (2006).

3 Results and discussions

It is well known that the temporal variations of the aerosol optical properties at different

177 wavelengths are generally consistent with each other. Therefore, only single-wavelength (such as 550
178 nm) AAC, SC, Bsp, SSA and ASP are focused when analyzing their basic characteristics (including
179 temporal variations, frequency distributions and changes with wind direction), their relationships with
180 each other, and their relationships with the meteorological conditions (such as RH and VIS) and
181 columnar AOD.

182 **3.1 Temporal variations of the aerosol optical properties**

183 The aerosol absorption coefficient (AAC) was directly obtained from the measurement of AE-31
184 and the scattering and backscattering coefficients (SC and Bsp), which were directly measured from
185 Aurora 3000. Based on wavelength-dependent AAC and SC, Ångström exponent of absorbing (AAE at
186 470/660 nm) and scattering (SAE at 450/635 nm) aerosols were estimated according Eq.5 and Eq. 6,
187 respectively. Based on AAC, SC and Bsp, wavelength-dependent aerosol asymmetry parameter (ASP),
188 single scattering albedo (SSA) and extinction coefficient (EC) are further estimated using Eqs. 8~10
189 and analyzed. Table 1 lists the statistical summary of surface aerosol optical properties in urban area of
190 Nanjing during the sampling period. The annual mean AAC, SC, Bsp, EC, SSA and ASP at 550 nm,
191 AAE at 470/660 nm and SAE at 450/635 nm is 29.615 Mm^{-1}, 338.275 Mm^{-1}, 44.257 Mm^{-1}, 381.958
192 Mm^{-1}, 0.901, 0.571, 1.583 and 1.320, respectively, with a standard deviation of 20.454 Mm^{-1}, 228.078
193 Mm^{-1}, 27.396 Mm^{-1}, 252.271 Mm^{-1}, 0.049, 0.088, 0.228 and 0.407, respectively.

194 **Table 1**

195 Figure 1 shows the 10th, 25th, median, 75th and 90th percentile values of the 550 nm- AAC, SC,
196 Bsp, 470/660 nm-AAE and 450/635 nm-SAE in urban area of Nanjing in each season from Mar 2014
197 to Feb 2016. Default values of aerosol scattering properties in spring 2014 are blank because the
198 measurements of Aurora 3000 started from June 2014. The figure suggests that AAC, SC, Bsp, AAE

and SAE have substantially seasonal variations. High level of AAC appears in winter (DJF) while the lower one is found in summer (JJA) (Fig. 1a). The temporal variability of Bsp is similar to that of AAC (Fig. 1d). According to Zhang et al. (2009), emissions of the aerosols and trace gases in China are larger in winter than in other seasons especially for carbonaceous aerosols (Fig. 1c in Zhuang et al., 2013b). Thus, the higher AAC values in winter than in summer might result from the higher aerosol emissions, lower boundary height (Guo et al., 2016b) and less rainfall. However, possibly due to the impacts of hygroscopic growth of aerosol caused by higher RH in summer and dust aerosol in spring (Zhuang et al., 2014a), SC is considerably large in these two seasons (Fig. 1c). Thus, the lowest SC is found in autumn in both 2014 and 2015. AAE has seasonality similar to AAC. Due to relatively higher RH, small value of AAE is found in JJA while the larger ones appear in the other seasons (Fig. 1b), which is different from the seasonality of SAE. SAE is larger in warmer seasons but is smaller in the other seasons. Scattering aerosols, including inorganic and partially organic components, mainly come from gas-to-particle transformation, so that they have smaller sizes (larger AE) compared to the primary aerosols (such as dust and BC). The efficiency of gas-to-particle transformation is higher in warmer seasons. The observations of the aerosol compositions at the site showed that seasonal mean inorganic aerosols, including sulfate, nitrate and ammonium, account for about 50% of the total $PM_{2.5}$ in spring and might be higher than 50% in the other seasons (Zhuang et al., 2014b). Thus, SAE in summer and autumn is large (Fig. 1e). RH can impose substantial influences on scattering aerosols. SAE might be much larger than the current values in these two seasons if the hygroscopic growth were excluded. Seasonal mean RH is about 75.41% and 70.86% in JJA and SON, respectively, to a certain degree leading to higher values of SAE in autumn than in summer. The figure also suggests that aerosol absorption coefficient and scattering coefficient as well as their sizes in 2014 are higher than those in

2015. The observed RH difference in these two years at least partly accounts for the variation of aerosol absorption coefficient and scattering coefficient as well as their sizes. A comparison of RH between 2014 and 2015 indicates that RH is 79.49% and 72.86% in JJA and SON, respectively, in 2014, larger than that in 2015 (71.33% in JJA and 69.03 in SON).

Figure 1

Figure 2 plots the seasonal mean values with standard deviations of AAC, SC, Bsp, EC, SSA, ASP, AAE at 470/660 nm and SAE at 450/635 nm. AAC, SC, Bsp and EC increase with decreasing wavelength in four seasons. Changes in SSA and ASP with increasing wavelength are different in different seasons. SSA increases with increasing wavelength in colder seasons but little in JJA and SON. ASP increases with wavelength in JJA, opposite to in other seasons. The figure also suggests that seasonal variation of EC is more consistent with SC's, with large values in JJA and DJF (370.236 and 422.569 Mm^{-1}, respectively, at 550 nm). The largest values of SSA and ASP appear in JJA (0.933 and 0.638, respectively, at 550 nm), implying that aerosols in urban area of Nanjing are more scattering and have stronger forward scattering ability in JJA than in other seasons. The urban aerosols are more absorbent in SON and DJF in Nanjing (550 nm SSA is no more than 0.89). Seasonal variation of SSA is determined by the variations of both AAC and SC. As mentioned above, AAC is the highest in winter while lowest in summer to a great degree due to the seasonality of the emissions. SC would have the same variation as AAC if only emissions were taken into account. Zhang et al. (2009) indicates that the emission seasonality of carbonaceous aerosols are much stronger than the trace gases (such SO_2 and NOx), and they shows that anthropogenic emission rate in winter is about 1.87 times to that in summer for black carbon while only about 1.2 for SO_2 in China. This is also supported by Sun et al. (2015), who found that concentration of black carbon aerosol in north China was much higher in winter due to

243 enhanced emissions based on 1 year observations. Thus, the different emission seasonal variations
244 between black carbon and trace gases alone would cause a lower SSA in winter compared to that in
245 summer. What's more, both higher efficiency of gas-to-particle transformation and higher level of RH
246 in summer are in favor of a much larger SC, which to a certain degree could further enlarge SSA in
247 summer. The smaller SSA in colder season might mainly be caused by a higher emission of absorbing
248 aerosol.

249 **Figure 2**

250 Seasonal mean 550 nm AAC, SC, Bsp, EC, SSA, and ASP, 470/660 nm AAE and 450/635 nm
251 SAE as well as corresponding standard deviations are listed in Table 2. It suggests that seasonal mean
252 550 nm AAC, SC, Bsp, EC, SSA, and ASP vary from 19.65 to 37.96 Mm^{-1}, 294.62 to 385.14 Mm^{-1},
253 36.99 to 54.79 Mm^{-1}, 341.3 to 422.57 Mm^{-1}, 0.874 to 0.933, and 0.54 to 0.64, respectively. Seasonal
254 mean AAE and SAE vary from 1.49 to 1.70 and 1.1 to 1.54, respectively. AAC and Bsp in DJF are
255 about 2 and 1.5 times of those in JJA, respectively. SSA in JJA is about 6.75% larger than that in SON.

256 **Table 2**

257 In addition to seasonality, the aerosol optical properties near the surface at urban Nanjing have
258 substantial diurnal variations (Figure 3), especially for the coefficients (AAC, SC, Bsp and EC). The
259 diurnal variation of EC, which is consistent with SC, is not showed in the figure. AAC levels are
260 usually high at the rush hours around 07:00-09:00 am and around 09:00-11:00 pm but low in the
261 afternoon (Fig. 3a). At 08:00 am, mean 550 nm-AAC is as large as about 34 Mm^{-1}, while at 02:00 pm,
262 it is about 23 Mm^{-1}. SC and Bsp (Fig. 3b and 3c), to some extent, have diurnal variations similar to
263 AAC's. Their lowest values also appear in the afternoon (about 280 Mm^{-1} for SC and 38 Mm^{-1} for Bsp).
264 However, only one peak of the aerosol scattering coefficient is found in the early morning (about 379

265 Mm^{-1} for Sc and 48 Mm^{-1} for Bsp) and it is about 1-2 hours earlier than its absorption coefficient
266 possibly owing to the different emissions between these two types of aerosols. Absorbing aerosols in
267 urban Nanjing mainly come from the vehicle emissions because of the developed transportation
268 network, resulting in two peaks of AAC within one day (Zhuang et al. 2015). Scattering aerosol
269 loadings are somewhat less affected by traffic emissions especially in nighttime. Their precursors, such
270 as SO_2 and NOx, mostly come from coal combustion and industrial emissions in urban Nanjing based
271 on source apportionment. Therefore, there is no peak for SC or Bsp before midnight, although their
272 values are considerably large (about 350 and 46 Mm^{-1}, respectively). Different diurnal cycles between
273 AAC and SC were also observed in sub-urban area of Nanjing (Yu et al., 2016). Diurnal variations of
274 AAC, SC and Bsp might be highly affected by the diurnal cycles of the boundary layer. The small
275 coefficients in afternoon are mostly induced by well developed mixing layer (Zhuang et al. 2014b).
276 Generally, the boundary layer becomes more and more stable after sunset and its height becomes lower,
277 which is conducive to the accumulation of air pollutants in the nighttime especially during the period
278 from midnight to sunrise. Therefore, SC usually peaks in early morning and the peak appears at
279 different times in different seasons (05:00 am in JJA and 08:00-09:00 am in DJF). The daytime peak of
280 AAC appears at 07:00 am in JJA and at 09:00 am in DJF. Diurnal variation of SSA also reflects the
281 difference between AAC and SC (Fig. 3d), implying that aerosols in urban Nanjing are more scattering
282 after midnight (SSA is about 0.91) while more absorbing before noon and midnight (SSA is about 0.89).
283 Scattering aerosols mainly come from strong chemical production (gas-to-particle transformation) at
284 daytime, which to some extent might offset the dilution effect of the boundary on SC, thus, leading to a
285 relatively larger SSA in afternoon. The figure further shows that both AAE (Fig. 3e) and SAE (Fig. 3f)
286 at daytime are slightly larger than those after midnight because both absorbing and scattering aerosols

are more fresher at daytime while they are more aged before sunrise. Diurnal variations of SAE and AAE are relatively weaker compared to corresponding coefficients. In addition to aerosol loadings, the level of Bsp is also affected by the size of the aerosols as suggested by Yu et al. (2016), so is ASP (Fig. 3g). Diurnal cycle of ASP is similar to that of Bsp but is opposite to that of SAE. Large ASP appears in early morning (0.587) and the lower ASP in afternoon (0.552).

Figure. 3

3.2 Frequencies of the aerosol optical properties

The frequency of the aerosol optical properties is presented in Figure 4 and Table 3. Similarly, the frequency of EC is not shown in the figure because it has similar pattern to SC's. Almost all of them follow a unimodal pattern. As listed in Table 3, the dominant ranges for all the aerosol optical properties are distributed around their annual mean values, respectively, with different widths and they account for at least 60% of the total samplings during the entire study period. The maximum frequencies of 32.9% (AAC), 24.04% (SC), 26.45% (Bsp), 18.64% (SSA), 20.9% (AAE), 18.06% (SAE) and 34% (ASP) occur in the ranges from 9 to 21 Mm^{-1}, 170 to 280 Mm^{-1}, 30 to 45 Mm^{-1}, 0.91 to 93, 1.5 to 1.6, 1.32 to 1.5 and 0.55 to 0.62, respectively. Frequency distributions of the aerosol optical properties have substantially seasonal variations. The frequency peaks of the properties would be more concentrated at lower/higher ranges if their seasonal means are smaller/larger. As shown in Fig. 4a, 4c, and 4e, relatively larger values or the peaks of frequencies for AAC, Bsp and AAE are concentrated in lower value ranges in JJA but in higher value ranges in the other seasons. Moisture absorption growth of absorbing aerosols leads to a left-ward shift in an AAE-frequency curve in JJA. Effects of dust aerosol also might result in a left-ward shift in a SC-frequency curve in spring (Fig. 4f). Furthermore, due to dust and RH, SC is considerably large in MAM and JJA, leading to relatively larger frequencies

of SC distributed at larger SC ranges compared with the ones of AAC. As mentioned above, aerosols in urban Nanjing are more scattering and have stronger forward scattering ability in JJA than in the other seasons, thus larger frequencies occur more at higher value ranges of SSA and ASP in JJA.

Figure 4

Table 3

3.3 Aerosol optical properties in different wind directions

East Asian monsoon is active in middle latitudes. Nanjing could be affected by East Asian summer monsoon in JJA and by the winter monsoon in DJF. Air flows in these two seasons are significantly different (Figure 5a and 5b) so to alter the aerosol optical properties in different seasons. Air masses mostly come from the oceans (about 77%) in JJA and from continental regions in north and northwest of China (57%) in DJF. Only a few percentages of air masses are from the north region of China in JJA. Additionally, considerable air masses arriving at the site are from the local areas (cluster 1 in JJA) or from places near Nanjing (cluster 1 in DJF). Therefore, the aerosol optical properties at the study site are characterized differently with different air masses in the two seasons.

As suggested by Zhuang et al. (2014b), high BC loadings in early June 2012 were observed at the site when the air masses were from northwestern directions of Nanjing, in which seriously biomass burning was detected. Therefore, the aerosol optical properties are further analyzed by their origins in both JJA and DJF (Fig 5c and 5d). In JJA, seasonal mean AAC, SC, Bsp, SSA, ASP, AAE and SAE are about 19.65 Mm^{-1}, 340.87 Mm^{-1}, 36.99 Mm^{-1}, 0.93, 0.64, 1.49 and 1.34, respectively (Table 2). The dominant air masses are from local areas (cluster 1 in Fig. a) and east ocean (on the way through urban agglomeration regions (cluster 2) and less-developed regions (cluster 3) of the Yangtze River Delta YRD), accounting for 90% of the total characteristics of the aerosol optical properties in urban Nanjing.

All the values of the properties in the first three clusters are more close to their season means. Aerosol absorption and scattering coefficients from local emissions are larger than those in the other clusters. Although air masses in cluster 2 and cluster 3 come from the oceans and have the same level of relative humidity (RH), differences still exist between the clusters. The air masses have to cross the urban agglomeration (from Shanghai to Nanjing) of YRD when they arrive Nanjing in cluster 2 but pass less developed regions (north Jiangsu Province) in cluster 3. In YRD, emissions of the aerosols and trace gases are much stronger in urban agglomeration regions than those in other area as suggested in Zhang et al. (2009) and Zhuang et al. (2013b). Therefore, AAC and SC in cluster 2 are larger than those in cluster 3 to some extent (Fig. 5a and 5c). Aerosols from these two clusters are more scattering than the local ones. There are two clusters (cluster 4 and 5 in Fig. 5a) from the remote areas in JJA. Aerosol loadings are relatively small when the air masses from these two clusters. The size of the aerosols is finer (larger AAE in cluster 5 and SAE in cluster 4 and 5 in Fig. 5c). ASP varying with the clusters coincides with RH varying with the clusters (Fig. 5c), implying that RH might influence ASP significantly. In DJF, seasonal mean AAC, SC, Bsp, SSA, ASP, AAE and SAE are about 37.96 Mm^{-1}, 385.14 Mm^{-1}, 54.79 Mm^{-1}, 0.89, 0.54, 1.70 and 1.24, respectively (Table 2). Similar to JJA, the aerosol absorption and scattering coefficients are the largest, all of which (AAC, SC and Bsp) are about 1.3 times of their season means (Fig. 5d), when the air masses are local or from the regions (cluster 1 in Fig. 5b) near Nanjing in DJF. AAC, SC, Bsp, SSA and ASP are small but AAE and SAE are large if air masses are from remote areas. Aerosols are the smallest, most absorbing and finest when the air masses are from near Lake Baikal. ASP varying with the clusters also coincides with RH varying with the clusters in this season (Fig. 5d), further implying the effect of RH on ASP.

Figure 5

353 Substantial studies on the aerosol optical properties have been carried out in China from monthly
354 to annual scales. Table 4 lists some annual and seasonal statistics of measured surface aerosol optical
355 properties from literature. Annual and season means listed in the table are comparable to some extent,
356 although the observational periods and instruments are different. It suggests that AACs and SCs in
357 urban areas are much higher than those in rural and remote areas. In Beijing (center of
358 Beijing-Tianjin-Hebei region), annual mean AAC and SC were 56 and 288 Mm^{-1} in urban site during
359 the period from 2005 to 2006 (He et al., 2009), which were much larger than the ones (17.5 and 174.6
360 Mm^{-1}, respectively) in rural area (Yan et al., 2008). In Chengdu (Tao et al., 2014), Xi'an (Cao et al.,
361 2012) and Wuhan (Gong et al., 2015), which is the center from southwest to central China, the annual
362 mean scattering coefficients in these cities exceeded 450, 520 and 370 Mm^{-1}, respectively. In Pearl
363 River Delta (PRD) region, seasonal mean AAC at 532 nm was about 84 and 188 Mm^{-1} at an urban site
364 (Panyu), about 47 and 95 Mm^{-1} at a suburban site (Dongguan), about 26 and 28 Mm^{-1} at a rural site,
365 and only 7.21 and 8.37 Mm^{-1} at a remote site (Yongxing Island), in spring and winter, respectively (Wu
366 et al., 2013). Additionally, aerosols in urban areas are more absorbing. The aerosol absorptions in urban
367 areas have stronger seasonality than those in rural areas (Table 4). Urban aerosols in Nanjing in annual
368 scale are somewhat lower but more scattering than those in most cities in China. In addition to annual
369 and seasonal means, there are considerable studies on monthly mean aerosol optical properties (e.g.,
370 Bergin et al., 2001; Xu et al., 2002; 2004; Li et al., 2007; Andreae et al., 2008; Li et al., 2015a; b). A
371 few studies on the aerosol optical properties in Nanjing have been carried out previously (Zhuang et al.,
372 2014a; 2015; Yu et al., 2016) based on observations. They were more focused on the columnar aerosols
373 (Zhuang et al., 2014a), or single optical property (Zhuang et al., 2015), or shorten observations (two
374 months in Yu et al., 2016). Substantial analysis in the key optical properties of the surface aerosol here

to a certain degree fill the gaps in the study on the aerosols in Nanjing, even in YRD.

Table 4

3.4 Relationship among aerosol optical properties, relative humidity and visibility

The relationships between SC and AAC, SC and Bsp are presented by season in Figure 6. As shown in Figures 3 and 4, these three types of coefficients have similar diurnal and frequency distributions. The linear correlation coefficient varies from 0.93 to 0.97 for SC and Bsp and from 0.66 to 0.87 for SC and AAC in urban Nanjing. It is obvious that relations between SC and Bsp are much better than those between SC and AAC in all seasons. The correlation between AAC and SC becomes poorer in MAM (0.66) and JJA (0.78) because the scattering aerosols are more affected by dust in spring and SC is more affected by RH in summer. The linear correlation coefficients between SC and AAC and between SC and Bsp in MAM at the site were a little smaller than that in suburban Nanjing (Yu et al., 2016) in the same season in 2011. The slope of the fitting between Bsp and SC represents the levels of ASP. Analysis (not shown) suggests that ASP has a significant anti-correlation with the ratio of Bsp to SC (linear R=-0.98). Thus, a greater slope of curve represents a smaller ASP, thus less forward scattering of the aerosols.

Figure 6

The correlations between ASP and SC under different RH conditions are illustrated in Figure 7, showing that ASP has a quasi-LogNormal distribution with SC especially in lower RH conditions. ASP increases monotonically with increasing SC in low RH ranges (Fig. 7a and 7b, RH < 60%) and ASP mostly concentrates at small SC regions when RH is less than 40% (Fig. 7a), implying that fine particles dominates the most in low RH conditions as also suggested by Andrews et al. (2006) and Badu et al. (2012). The correlation between ASP and SC becomes poorer with increasing RH (Fig. c),

397 indicating that both fine and coarse aerosols might be equally important to the total SC.

398 **Figure 7**

399 Figure 8 shows the relationships between the SSA at 491 nm and extinction Angstrom exponent
400 (EAE) at 491/863 nm (Fig. a) as well as between SSA difference (863 nm - 491 nm) (short for dSSA)
401 and EAE at 491/863 nm (Fig. b). Overall, SSA or dSSA to a certain degree have an anti-correlation
402 with EAE in urban area of Nanjing, especially for the latter one. Linear correlation coefficient is about
403 -0.13 between SSA and EAE and about -0.75 between dSSA and EAE. Relationships between the SSA
404 (or dSSA) and EAE to some extent reflect the aerosol types and sources as indicated by Russell et al.
405 (2014), who proposed a method to identify the aerosol types based on the columnar aerosol optical
406 properties (including SSA, EAE and the real refractive index) from the Aerosol Robotic Network
407 (AERONET) retrievals. They suggested that: 1. The polluted dust aerosol had smaller EAE (near 1.0)
408 and SSA ranged from 0.85 to 0.95. 2. The urban aerosols had larger EAE values (around 1.4) and SSA
409 ranges (0.86~1.0) compared with the dust aerosols. 3. The biomass burning aerosol (dark type) had the
410 largest EAE (exceeding 1.5) while smaller SSA (about 0.85). If there were two kind of aerosols having
411 nearly identical coordinates in SSA and EAE, further information (such as the real refractive index)
412 should be used (Russell et al., 2014). Based on this method, the figure further implies that, in addition
413 to local emissions, aerosols in urban area of Nanjing might also be affected substantially by the
414 long-distance transported dust (or polluted dust) in spring and be influenced to some extent by biomass
415 burning in fall.

416 **Figure 8**

417 Atmospheric humidity has significant influences on the growth of particulate matter, subsequently
418 affecting the sizes and absorbing/scattering abilities of the aerosols. As shown in Figure 7a and 7c, high

levels of SC are likely found in high RH ranges. Seasonal mean RH is the largest in summer but lowest in winter (Figure 9a). In summer, both trace gases and particulate matters have lower emission rates as suggested by Zhang et al. (2009). Furthermore, PBL height and precipitation mostly have larger values in this season than those in other seasons. Thus, these three factors would result in smaller aerosol loadings in summer (such as Bsp is the smallest in this season). However, different from Bsp, SC in summer is larger than that in spring and fall, which might mainly result from the effects of high RH (Fig. 1c and 1d) although gas-to-particle transformation also have contribution to SC to a certain degree in this season. Zhang et al. (2015) indicated that SC and Bsp in YRD would increase by 50% and 25% as the RH increased from 40% to 85% and the increment would become larger if there were considerable amount of nitrate in fine particles. And nitrate in urban area of Nanjing accounts for more than 20% (as much as sulfate) of the total $PM_{2.1}$ (Zhuang et al., 2014a). RH might also affect the sizes of the aerosol. The smallest AAE in JJA always corresponds to the highest RH, and vice versa (Fig. 1b and 9a). These results are consistent with Zhuang et al. (2014a), in which characteristic of columnar aerosol optical properties were investigated. Figure 9b further shows that AAE and SAE decrease monotonically with increasing RH. The correlation between ASP and RH is opposite to that between aerosol Ångström exponent and RH. The linear correlation coefficients are -0.36, -0.15 and 0.6 between AAE and RH, SAE and RH, and ASP and RH, respectively, in urban areas of Nanjing. ASP and RH are highly correlated with each other, which are also reflected in Fig. 2f, Fig. 5c, Fig. 5d and Fig. 9a, implying that RH might have considerable influence on the aerosol forward scattering coefficient hence SC. These results could be used to correct the aerosol optical parameters in numerical models for estimating the aerosol radiative forcing in East China as suggested by Andrews et al. (2006), in hope to reduce uncertainties in such estimation.

441 **Figure 9**

442 High levels of aerosol loadings would directly affect the visibility (VIS), which is one of the
443 factors being concerned about in current air quality forecasting in China. The forecast accuracy of
444 visibility or haze pollutions would be increased significantly if the effects of aerosols on visibility can
445 be figured out. Instead of the loadings of the particulate matter, the aerosol optical properties here are
446 used when investigating the aerosol effects on VIS.

447 Figure 10 shows the relations between extinction coefficient (EC) and VIS and between SC and
448 VIS by season under different RH levels. Atmospheric VIS is found to decrease exponentially with
449 increasing EC or SC in all seasons. The lapse rate of VIS with EC or SC is much larger in spring and
450 summer than in fall and winter. The lower VIS always appears at higher RH ranges, and vice versa. In
451 small VIS regions (such as: <4 km), VIS values are much smaller in JJA than those in the other seasons
452 under the same SC level, implying the strong effects of RH on VIS. The effect of AAC on VIS has
453 substantial seasonality and it is strong in SON but weak in MAM and JJA as illustrated in the fitting
454 lines in the figure. Study on the effects of PM on VIS might be more reasonable if using the aerosol
455 optical properties rather than its mass concentrations. The linear correlation coefficient between EC and
456 VIS varies from -0.69 (in JJA) to -0.87 (in DJF), and between SC and VIS, it varies from -0.71 (in JJA)
457 to -0.87 (in DJF) in urban area of Nanjing.

458 **Figure 10**

459 In addition to the SC or EC, the aerosol SSA and ASP also have good relationships with VIS as
460 shown in Figure 11, in which the effects of RH and SAE are also included (larger markers represent
461 smaller SAE, but larger size of the aerosols). The aerosols would become coarser, less absorbing and
462 more forward scattering to some extent with increasing RH, which subsequently further exacerbate the

463 deterioration of visibility in all the seasons. The linear correlation coefficients vary from -0.48 (in JJA)
464 to -0.73 (in SON) between SSA and VIS and -0.47 (in JJA) to -0.80 (in MAM) between ASP and VIS
465 in urban Nanjing. These results additionally illustrate that the scattering aerosols are still the key factors
466 affecting the atmospheric visibility, although the absorbing aerosols might have considerable influences
467 on VIS in some seasons (Fig. 10c). The results in this study further indicate that effects of aerosols on
468 air quality are complex.

469 **Figure 11**

470 Comparison between surface aerosol extinction coefficient and columnar AOD is performed
471 (Figure 12). Differences exist between EC and AOD, although they are well correlated with each other
472 in each season. AOD to some extent is less affected by the development of boundary layer and more
473 affected by the transport of aerosols compared to EC at the surface. The seasonal mean EC is large both
474 in JJA and in DJF while the largest AOD is only found in JJA, which is possibly related to higher
475 boundary layer height in JJA. A lower boundary layer would lead to more aerosol accumulation at the
476 surface thus result in its smaller column burden. These differences (high surface aerosol loadings but
477 low AOD) have also been simulated by a regional climate chemistry model in Zhuang et al. (2011 and
478 2013). Overall, high AOD level corresponds to large EC value in each season, implying that aerosols in
479 the upper layers mostly come from surface emissions in urban Nanjing. In some cases, long distance
480 transport of aerosols might contributes significantly to the AOD as shown in Fig. 12a, in which AOD
481 exceeds 2 meanwhile EC is found to appear in low value ranges. The slope of the linear fitting is larger
482 in JJA (about 0.0016) than that in the other seasons (all about 0.001), indicating that for a given value
483 of EC, AOD would be higher in JJA possibly because of higher humidity in summer. The columnar
484 water vapor in summer is about 2 to 5 times of that in the other seasons.

Figure 12

4 Conclusions

In this study, the near-surface aerosol optical properties, including aerosol scattering (SC), back scattering (Bsp), absorption (AAC) and extinction (EC) coefficients, single scattering albedo (SSA), scattering (SAE) and absorbing (AAE) Ångström exponent, as well as asymmetry parameter (ASP), are investigated based on the measurements with the 7-channel Aethalometer (model AE-31, Magee Scientific, USA) and three-wavelength integrating Nephelometer (Aurora 3000, Australia) in urban area of Nanjing.

In urban area of Nanjing, the annual mean EC, SSA and ASP at 550 nm are 381.958 Mm^{-1}, 0.901, 0.571, respectively. SC, which accounts for about 90% of EC, is about one order of magnitude larger than AAC, implying that EC to a great degree has similar temporal variation and frequency distribution to SC. Absorbing aerosol is finer than the scattering one. AAE at 470/660 nm is about 1.58, about 0.2 larger than SAE. All of them above have substantially seasonal and diurnal variations. Both the aerosol absorption and scattering coefficients have the largest values in winter due to the higher emissions. However, SC also has a higher values in summer and spring likely due to higher relative humidity (RH) and efficiency of gas-to-particle transformation in summer and the effect of dust in spring, respectively. High RH in summer results in the lowest AAE and largest ASP being found and it is also lead to a relatively smaller SAE, although a large number of fine scattering aerosols could be produced through intensive gas-to-particle transformation in this season. Seasonality of SSA is co-determined by AAC and SC, showing the largest value in summer and lowest value in fall. AAC, SC, Bsp and EC have more substantial diurnal variations than SSA, AAE, SAE and ASP. Because of traffic emissions, AACs are high at the rush hours (around 09:00 am and pm) but low in afternoon when the boundary layer

being well developed. SC and Bsp usually peak in the early morning before sunrise (1-2 earlier than AAC's) and reach the bottom in the afternoon. High levels of SC and Bsp are mostly caused by accumulation of air pollution in the nighttime from midnight to sunrise. The diurnal variation of SSA is also depended on AAC and SC. SSA is large after midnight and noon. AAE and SAE at daytime are slightly larger than after midnight because both absorbing and scattering aerosols are fresher at daytime but more aged before sunrise. ASP, which is related to the size of the aerosols, its diurnal variation is opposite to SAE's but similar to Bsp's.

The seasonal and diurnal observations on the aerosol optical properties are of great importance to the modeling community. In addition to the aerosol emission rates, compositions, mixing states, and profiles, uncertainties of the aerosol seasonality and diurnal variations might also lead to large bias when investigating the aerosol radiative forcing and climate effects. Xu et al. (2016) presented that the aerosol direct radiative forcing would be underestimated both at the TOA and surface by 2.0 and 38.8 W/m^2, respectively, if the diurnal variation were excluded. Large bias of the aerosol forcing would subsequently result in substantial uncertainties of the climate responses to the aerosol. Analysis on the seasonal and diurnal variations of the aerosol optical properties in this study to some extent are valuable to the modeling-based researches on the aerosol climate effects.

Frequency analysis indicates that almost all of the aerosol optical properties follow a unimodal pattern in urban area of Nanjing. The ranges around their averages, with different widths, account for more than 60% of the total samplings. Frequency distributions of the aerosol optical properties also have substantial seasonality. The frequency peak of a property would be more concentrated among lower/higher ranges if the seasonal mean is smaller/larger. Back trajectory analysis suggests that the source of aerosols in Nanjing are mainly from the local and regional emissions around YRD in summer,

while from the sources include both local emissions and transport from central and north China in winter. In JJA, aerosols are more scattering when air masses come from the East China Sea and finer if air masses come from remote areas. In DJF, AAC, SC, Bsp, SSA and ASP are low while AAE and SAE are high in urban Nanjing under the conditions of air masses being transported from remote areas. ASP varied with the clusters is consistent with RH in both JJA and DJF.

The correlation between SC and Bsp is much better than that between SC and AAC in all seasons. In spring, these relationships are a little weaker than those in suburban Nanjing. ASP has a quasi-LogNormal distribution with SC under a condition of RH being lower than 60%, increasing monotonically with increasing SC. It would be mostly concentrated at small SC regions when RH is less than 40% because finer particles dominant under low RH conditions. The correlation between ASP and SC becomes weaker with increasing RH, indicating that both fine and coarse aerosols might be equally important to the total SC in high RH conditions. Atmospheric humidity can significantly modulate aerosol optical properties. Due to the effects of RH in summer, the aerosol would become coarser and its forward scattering efficiency would be stronger with increasing in RH. The linear correlation coefficients are -0.36, -0.15 and 0.6 between AAE and RH, SAE and RH, and ASP and RH, respectively, in urban areas of Nanjing. Comparisons also indicate that seasonal variation of surface aerosol EC (high in JJA and DJF) is different from its columnar optical depth (AOD, high in JJA and low in DJF), even though they are closely correlated to each other within each season. Overall, high AOD level corresponding to large EC value in each season implies that aerosols in upper layers are mostly from surface emissions. AOD would be higher in JJA than in other seasons in a condition with fixed EC, possibly due to the effects of high humidity.

Overall, the scattering aerosols are still the key factor in affecting the atmospheric visibility

(VIS), although the absorbing aerosol has considerable contributions in some seasons. The linear correlation coefficient between EC and VIS varies from -0.69 to -0.87, close to those between SC and VIS. VIS is found to be decreased exponentially with increasing EC or SC in all seasons. And its lapse rate along with EC or SC is much larger in spring and summer than in fall and winter. In small VIS regions (i.e., VIS<4 km), VIS values are much smaller in JJA than in other seasons if the SC levels are the same, further indicating the strong effect of RH on VIS. The aerosol SSA and ASP could also affect VIS. Large SSA and ASP might further exacerbate the deterioration of visibility. The linear correlation coefficients between seasonal SSA and VIS varies from -0.48 to -0.73 and from -0.47 to -0.80 between ASP and VIS in urban area of Nanjing.

Acknowledgements: This work was supported by the National Key Basic Research Development Program of China (2014CB441203, 2016YFC0203303), the National Natural Science Foundation of China (41675143, 91544230, 41621005), FP7 project: REQUA (PIRSES-GA-2013-612671), and a project Funded by the Priority Academic Program Development of the Jiangsu Higher Education Institutions (PAPD). the National Science Foundation of Jiangsu Provence (Grant #BE2015151). The authors would like to thank all members in the AERC of Nanjing University for maintaining instruments, and also thank the anonymous reviewers for their constructive and valuable comments on this paper. The HYSPLIT model was supplied by NOAA: http://ready.arl.noaa.gov/HYSPLIT_traj.php.

5 References

Andreae, M. O., Schmid, O., Yang, H., Chand, D., Yu, J. Z., Zeng, L. M., and Zhang, Y. H.: Optical properties and chemical composition of the atmospheric aerosol in urban Guangzhou, China Atmos. Environ., 42, 6335–6350, 2008.

Andrews, E., Sheridan, P. J., Fiebig, M., McComiskey, M., Ogren, J. A., Arnott, P., Covert, D., Elleman, R., Gasparini, R., Collins, D., Jonsson, H., Schmid, B., and Wang, J.: Comparison of methods for deriving aerosol asymmetry parameter, J. Geophys. Res., 111, D05S04, doi:10.1029/2004JD005734, 2006.

Arnott, W. P., Hamasha, K., Moosmuller, H., Sheridan, P. J., and Ogren, J. A.: Towards aerosol light-absorption measurements with a 7-wavelength aethalometer: evaluation with a photoacoustic instrument and 3-wavelength nephelometer, Aerosol Sci. Tech., 39, 17–29, doi:10.1080/027868290901972, 2005.

Babu, S., Gogoi, M., Kumar, V. H. A., Nair, V. S., Moorthy, K. K.: Radiative properties of Bay of Bengal aerosols: spatial distinctiveness and source impacts, J. Geophys. Res., 117, D06213, doi:10.1029/2011JD017355, 2012.

Bai, H. T., Chen, Y. H., Wang, H. Q., Zhang, Q., Guo, N., Wang, S., Pan, H., and Zhang, P.: Seasonal variation of aerosol optical properties at AERONET of the semi-arid region in Loess Plateau, Arid Land Geogr., 34, 1–8, 2011.

Bellouin, N., Boucher, O., Tanré, D., and Dubovik, O.: Aerosol absorption over the clear-sky oceans deduced from POLDER-1 and AERONET observations, Geophys. Res. Lett., 30, 1748, doi:10.1029/2003GL017121, 2003.

Bergin, M. H., Cass, G. R., Xu, J., Fang, C., Zeng, L., Yu, T., Salmon, L. G., Kiang, C. S., Tang, X. Y.,

591 Zhang, Y. H., and Chameides, W. L.: Aerosol radiative, physical, and chemical properties in Beijing
592 during June 1999, J. Geophys. Res., 106 (D16), 17969–17980, 2001.
593 Cai, H. K., Zhou, R. J., Fu, Y. F., Zheng, Y. Y., and Wang, Y. J.: Cloud-aerosol lidar with or thogonal
594 polarization detection of aerosol optical properties after a crop burning case, Clim. Environ. Res.,
595 16, 469–478, 2011.
596 Cao, J., Wang, Q., Chow, J. C., Watson, J. G., Tie, X., Shen, Z., Wang, P., and An Z.: Impacts of aerosol
597 compositions on visibility impairment in Xi'an, China, Atmos. Environ., 59, 559–566, 2012.
598 Chameides, W. L., and Bergin, M.: Soot takes center stage, Science, 297 (5590), 2214-2215, 2002.
599 Che, H. Z., Zhang, X. Y., Xia, X., Goloub, P., Holben, B., Zhao, H., Wang, Y., Zhang, X. C., Wang, H.,
600 Blarel, L., Damiri, B., Zhang, R., Deng, X., Ma, Y., Wang, T., Geng, F., Qi, B., Zhu, J., Yu, J., Chen,
601 Q., and Shi, G..: Ground-based aerosol climatology of China: aerosol optical depths from the China
602 Aerosol Remote Sensing Network (CARSNET) 2002–2013, Atmos. Chem. Phys., 15, 7619–7652,
603 2015.
604 Cheng, Y. F., Wiedensohler, A., Eichler, H., Su, H., Gnauk, T., Bruggemann, E., Herrmann, H.,
605 Heintzenberg, J., Slanina, J., Tuch, T., Hu, M., and Zhang, Y. H.: Aerosol optical properties and
606 related chemical apportionment at Xinken in Pearl River Delta of China, Atmos. Environ., 42,
607 6351–6372, 2008.
608 Collaud Coen, M., Weingartner, E., Apituley, A., Ceburnis, D., Fierz-Schmidhauser, R., Flentje, H.,
609 Henzing, J. S., Jennings, S. G., Moerman, M., Petzold, A., Schmid, O., and Baltensperger, U.:
610 Minimizing light absorption measurement artifacts of the Aethalometer: evaluation of five
611 correction algorithms, Atmos. Meas. Tech., 3, 457–474, doi:10.5194/amt-3-457-2010, 2010.
612 Fan, X. H., Chen, H. B., Xia, X. A., Li, Z. Q., and Cribb, M.: Aerosol optical properties from the

613 Atmospheric Radiation Measurement Mobile Facility at Shouxian. China, J. Geophys. Res., 115,
614 D00K33, doi:10.1029/2010JD014650, 2010.
615 Forster, P., Ramaswamy, V., Artaxo, P., Berntsen, T., Betts, R., Fahey, D. W., Haywood, J., Lean, J.,
616 Lowe, D. C., Myhre, G., Nganga, J., Prinn, R., Raga, G., Schulz, M., and Van Dorland, R.: Changes
617 in atmospheric constituents and in radiative forcing, in: Climate Change 2007: The Physical
618 Science Basis. Contribution of Working Group I to the Fourth Assessment Report of the
619 Intergovernmental Panel on Climate Change, edited by: Solomon, S. et al., Cambridge Univ. Press,
620 Cambridge, UK, 129–234, 2007.
621 Gong, W., Zhang, M., Han, G., Ma, X., and Zhu, Z.: An investigation of aerosol scattering and
622 absorption properties in Wuhan, Central China, Atmosphere, 6, 503–520, 2015.
623 Guo, J., Miao, Y., Zhang, Y., Liu, H., Li, Z., Zhang, W., He, J., Lou, M., Yan, Y., Bian, L., and Zhai,
624 P.: The climatology of planetary boundary layer height in China derived from radiosonde and
625 reanalysis data, Atmos. Chem. Phys. Discuss., doi:10.5194/acp-2016-564, 2016b.
626 Guo, J., M. Deng, S. S. Lee, F. Wang, Z. Li, P. Zhai, H. Liu, W. Lv, W. Yao, and X. Li: Delaying
627 precipitation and lightning by air pollution over the Pearl River Delta. Part I: Observational
628 analyses, J. Geophys. Res. Atmos., 121, 6472–6488, doi:10.1002/2015JD023257.2016a.
629 Guo, J.P., X. Zhang, H. Che, S. Gong, X. An, C.X. Cao, J. Guang, H. Zhang, Y.Q. Wang, X.C. Zhang,
630 P. Zhao, X.W. Li: Correlation between PM Concentrations and Aerosol Optical Depth in Eastern
631 China, Atmospheric Environment, 43(37): 5876-5886. 2009.
632 He, X., Li, C. C., Lau, A. K. H., Deng, Z. Z., Mao, J. T., Wang, M. H., and Liu, X. Y.: An intensive
633 study of aerosol optical properties in Beijing urban area, Atmos. Chem. Phys., 9, 8903–8915,
634 doi:10.5194/acp-9-8903-2009, 2009.

635 Holler, R., Ito, K., Tohno, S., and Kasahara, M.: Wavelength-dependent aerosol single scattering albedo:
636 measurements and model calculations for a coastal site near the sea of Japan during ACE-Asia, J.
637 Geophys. Res., 108, 8648, doi:10.1029/2002JD003250, 2003.
638 IPCC, 2013: Climate Change 2013: The Physical Science Basis. Contribution of Working Group I to
639 the Fifth Assessment Report of the Intergovernmental Panel on Climate Change [Stocker, T.F., D.
640 Qin, G.-K. Plattner, M. Tignor, S.K. Allen, J. Boschung, A. Nauels, Y. Xia, V. Bex and P.M.
641 Midgley (eds.)]. Cambridge University Press, Cambridge, United Kingdom and New York, NY,
642 USA, 1535 pp.
643 Jacobson, M. Z.: Control of fossil-fuel particulate black carbon and organic matter, possibly the most
644 effective method of slowing global warming, J. Geophys. Res., 107, 4410,
645 doi:10.1029/2001JD001376, 2002.
646 Kiehl, J. T. and Briegleb, B. P.: The relative roles of sulfate aerosols and greenhouse gases in climate
647 forcing, Science, 260, 311–314, 1993.
648 Li, C., Marufu, L. T., Dickerson, R. R., Li, Z., Wen, T., Wang, Y., Wang, P., Chen, H., and Stehr, J. W.:
649 In situ measurements of trace gases and aerosol optical properties at a rural site in northern China
650 during East Asian Study of Tropospheric Aerosols: An International Regional Experiment 2005, J.
651 Geophys. Res., 112, D22S04, doi:10.1029/2006JD007592, 2007.
652 Li, J., Liu, X., Yuan, L., Yin, Y., Li, Z., Li, P., Ren, G., Jin, L., Li, R., Dong, Z., Li, Y., and Yang, J.:
653 Vertical distribution of aerosol optical properties based on aircraft measurements over the Loess
654 Plateau in China, J. Environ. Sci, 34, 44-56, 2015a.
655 Li, J., Yin, Y., Li, P., Li, Z., Li, R., Cribb, M., Dong, Z., Zhang, F., Li, J., Ren, G., Jin, L., and Li, Y.:
656 Aircraft measurements of the vertical distribution and activation property of aerosol particles over

the Loess Plateau in China, Atmos. Res., 155, 73–86, 2015b.

Li, Z., C. Li, H. Chen, et al.: East Asian Studies of Tropospheric Aerosols and their Impact on Regional Climate (EAST-AIRC): An overview. J. Geophys. Res. 116, D7, doi:10.1029/2010jd015257.2011.

Li, Z. Q., Lee, K. H., Wang, Y. S., Xin, J. Y., and Hao, W. M.: First observation-based estimates of cloud-free aerosol radiative forcing across China, J. Geophys. Res., 115, D00K18, doi:10.1029/2009JD013306, 2010.

Liao, H. and Seinfeld, J. H.: Global impacts of gas-phase chemistry-aerosol interactions on direct radiative forcing by anthropogenic aerosols and ozone, J. Geophys. Res., 110, D18208, doi:10.1029/2005JD005907, 2005.

Menon, S., Hansen, J., Nazarenko, L., and Luo, Y. F.: Climate effects of black carbon aerosols in China and India, Science, 297, 2250–2253, doi:10.1126/science.1075159, 2002.

Penner, J. E., Andreae, M., Annegarn, H., Barrie, L., Feichter, J., Hegg, D., Jayaraman, A., Leaitch, R., Murphy, D., Nganga, J., and Pitari, G.: Aerosols, their direct and indirect effects, in: Climate Change 2001: The Scientific Basis. Contribution of Working Group I to the Third Assessment Report of the Intergovernmental Panel on Climate Change, edited by: Houghton, J. T. et al., Cambridge University Press, Cambridge, UK and New York, NY, USA, 289–348, 2001.

Petzold, A., Kopp, C., and Niessner, R.: The dependence of the specific attenuation cross-section on black carbon mass fraction and particle size, Atmos. Environ., 31, 661–672, 1997.

Qian, Y., Gong, D.Y., Fan, J.W., Leung, L.R., Bennartz, R., Chen, D.L., Wang, W.G.: Heavy pollution suppresses light rain in China: Observations and modeling. J. Geophys. Res. 114, D00K02, doi:10.1029/2008jd011575. 2009.

Qin, S. G., Tang J, Wen YP (2001) Black carbon and its importance in climate change studies.

679 Meteorol Monogr 27(11):3–7.

680 Rosenfeld, D., Lohmann, U., Raga, G.B., O'Dowd, C.D., Kulmala, M., Fuzzi, S., Reissell, A., Andreae,

681 M.O.: Flood or drought: how do aerosols affect precipitation? Science 321, 5894, 1309-1313.

682 2008.Russell, P. B., Kacenelenbogen, M., Livingston, J. M., Hasekamp, O. P., Burton, S. P.,

683 Schuster, G. L., Johnson, M. S., Knobelspiesse, K. D., Redemann, J., Ramachandran, S., and

684 Holben, B.: A multiparameter aerosol classification method and its application to retrievals from

685 spaceborne polarimetry, J. Geophys. Res. Atmos., 119, 9838–9863, doi:10.1002/2013JD021411,

686 2014.

687 Schmid, O., Artaxo, P., Arnott, W. P., Chand, D., Gatti, L. V., Frank, G. P., Hoffer, A., Schnaiter, M., and

688 Andreae, M. O.: Spectral light absorption by ambient aerosols influenced by biomass burning in the

689 Amazon Basin. I: Comparison and field calibration of absorption measurement techniques, Atmos.

690 Chem. Phys., 6, 3443–3462, doi:10.5194/acp-6-3443-2006, 2006.

691 Streets, D. G., Gupta, S., Waldhoff, S. T., Wang, M. Q., Bond, T. C., and Bo, Y. Y.: Black carbon

692 emissions in China, Atmos. Environ., 35, 4281–4296, doi:10.1016/S1352-2310(01)00179-0, 2001.

693 Sun, Y. L., Wang, Z. F., Du, W., Zhang, Q., Wang, Q. Q., Fu, P. Q., Pan, X. L., Li, J., Jayne, J., and

694 Worsnop, D. R.: Long-term real-time measurements of aerosol particle composition in Beijing,

695 China: seasonal variations, meteorological effects, and source analysis, Atmos. Chem. Phys., 15,

696 10149-10165, doi:10.5194/acp-15-10149-2015, 2015.

697 Tao, J., Zhang, L. M., Cao, J. J., Hsu, S. C., Xia, X. G., Zhang, Z. S., Lin, Z. J., Cheng, T. T., and Zhang,

698 R. J.: Characterization and source apportionment of aerosol light extinction in Chengdu, southwest

699 China, Atmos. Environ., 95, 552–562, 2014.

700 Wang, T. J., Zhuang, B. L., Li, S., Liu, J., Xie, M., Yin, C. Q., Zhang, Y., Yuan, C., Zhu, J. L., Ji, L. Q.,

and Han, Y.: The interactions between anthropogenic aerosols and the East Asian summer monsoon using RegCCMS, J. Geophys. Res. Atmos., 120, doi:10.1002/2014JD022877, 2015.

Wang, Y., Che, H. Z., Ma, J. Z., Wang, Q., Shi, G. Y., Chen, H. B., Goloub, P., and Hao, X. J.: Aerosol radiative forcing under clear, hazy, foggy, and dusty weather conditions over Beijing, China, Geophys. Res. Lett., 36, L06804, doi:10.1029/2009GL037181, 2009.

Wang, Y., Wang, M., Zhang, R., et al., 2014. Assessing the effects of anthropogenic aerosols on Pacific storm track using a multiscale global climate model. Proceedings of the National Academy of Sciences 111, 19, 6894-6899.

Weingartner, E., Saathoff, H., Schnaiter, M., Streit, N., Bitnar, B., and Baltensperger, U.: Absorption of light by soot particles: determination of the absorption coefficient by means of aethalometers, J. Aerosol Sci., 34, 1445–1463, doi:10.1016/S0021-8502(03)00359-8, 2003.

Wu, D., Mao, J. T., Deng, X. J., Tie, X. X., Zhang, Y. H., Zeng, L. M., Li, F., Tan, H. B., Bi, X. Y., Huang, X. Y., Chen, J., and Deng, T.: Black carbon aerosols and their radiative properties in the Pearl River Delta region, Sci. China Ser. D, 52, 1152–1163, doi:10.1007/s11430-009-0115-y, 2009.

Wu, D.,Wu, C., Liao, B., Chen, H.,Wu, M., Li, F., Tan, H., Deng, T., Li, H., Jiang, D., and Yu, J. Z.: Black carbon over the South China Sea and in various continental locations in South China, Atmos. Chem. Phys., 13, 12257–12270, doi:10.5194/acp-13-12257-2013, 2013.

Wu, Y. F., Zhang, R. J., Pu, Y. F., Zhang, L. M., Ho, K. F., and Fu, C. B.: Aerosol optical properties observed at a semi-arid rural site in northeastern China, Aerosol Air Qual. Res., 12, 503–514, 2012.

Xia, X. A., Li, Z. Q., Holben, B., Wang, P., Eck, T., Chen, H. B., Cribb, M., and Zhao, Y. X.: Aerosol optical properties and radiative effects in the Yangtze Delta region of China, J. Geophys. Res., 112, D22S12, doi:10.1029/2007JD008859, 2007.

723 Xiao, Z. Y., Jiang, H., Chen, J., Wang, B., and Jiang, Z. S.: Monitoring the aerosol optical properties
724 over Hangzhou using remote sensing data, Acta Sci. Circumst., 31, 1758–1767, 2011.
725 Xin, J., Wang, Y., Pan, Y., et al.: The Campaign on Atmospheric Aerosol Research Network of China:
726 CARE-China. Bulletin of the American Meteorological Society 96, 7, 1137-1155,
727 doi:10.1175/BAMS-D-14-00039.1. 2014.
728 Xu, J., Bergin, M. H., Greenwald, R., Schauer, J. J., Shafer, M. M., Jaffrezo, J. L., and Aymoz, G.:
729 Aerosol chemical, physical, and radiative characteristics near a desert source region of Northwest
730 China during ACE-Asia, J. Geophys. Res., 109, D19S03, doi:10.1029/2003JD004239, 2004.
731 Xu, J., Bergin, M. H., Yu, X., Liu, G., Zhao, J., Carrico, C. M., and Baumann, K.: Measurement of
732 aerosol chemical, physical and radiative properties in the Yangtze delta region of China, Atmos.
733 Environ., 36, 161–173, 2002.
734 Xu, J., Tao, J., Zhang, R., Cheng, T., Leng, C., Chen, J., Huang, G., Li, X., and Zhu, Z.: Measurements
735 of surface aerosol optical properties in winter of Shanghai, Atmos. Res., 109-110, 25–35, 2012.
736 Yan, P., Tang, J., Huang, J., Mao, J. T., Zhou, X.J., Liu, Q., Wang, Z. F., and Zhou, H. G.: The
737 measurement of aerosol optical properties at a rural site in Northern China, Atmos. Chem. Phys., 8,
738 2229–2242, doi:10.5194/acp-8-2229-2008, 2008.
739 Yan, P.: Study on the aerosol optical properties in the background regions in the East part of China,
740 PhD Thesis, Peking University, China, 2006.
741 Yu, X. N., Ma, J., Kumar, K. R., Zhu, B., An, J. L., He, J. Q., and Li, M.: Measurement and analysis of
742 surface aerosol optical properties over urban Nanjing in the Chinese Yangtze River Delta, Sci. Total
743 Environ., 542, 277-291, 2016.
744 Zhang, L., Sun, J. Y., Shen, X. J., Zhang, Y. M., Che, H., Ma, L. Q., Zhang, Y. W., Zhang, X. Y., and

745 Ogren, J. A.: Observations of relative humidity effects on aerosol light scattering in the Yangtze
746 River Delta of China, Atmos. Chem. Phys., 15, 8439–8454, 2015.
747 Zhang, Q., Streets, D. G., Carmichael, G. R., He, K. B., Huo, H., Kannari, A., Klimont, Z., Park, I. S.,
748 Reddy, S., Fu, J. S., Chen, D., Duan, L., Lei, Y., Wang, L. T., and Yao, Z. L.: Asian emissions in
749 2006 for the NASA INTEX-B mission, Atmos. Chem. Phys., 9, 5131–5153,
750 doi:10.5194/acp-9-5131-2009, 2009.
751 Zhang, W., Hu, B., Chen, C. H., Du, P., Zhang, L., and Feng, G. H.: Scattering properties of
752 atmospheric aerosols over Lanzhou City and applications using an integrating nephelometer, Adv.
753 Atmos. Sci., 21(6), 848–856, 2004.
754 Zhang, X. Y., Wang, Y. Q., Niu, T., Zhang, X. C., Gong, S. L., Zhang, Y. M., and Sun, J. Y.:
755 Atmospheric aerosol compositions in China: Spatial/temporal variability, chemical signature,
756 regional haze distribution and comparisons with global aerosols, Atmos. Chem. Phys., 12, 779–799,
757 doi:10.5194/acp-12-779-2012, 2012.
758 Zhu, J., Wang, T., Talbot, R., Mao, H., Hall, C. B., Yang, X., Fu, C., Zhuang, B., Li, S., Han, Y., and
759 Huang, X.: Characteristics of atmospheric Total Gaseous Mercury (TGM) observed in urban
760 Nanjing, China, Atmos. Chem. Phys., 12, 12103–12118, doi:10.5194/acp-12-12103-2012, 2012.
761 Zhuang, B. L., Jiang, F., Wang, T. J., Li, S., and Zhu, B.: Investigation on the direct radiative effect of
762 fossil fuel black-carbon aerosol over China, Theor. Appl. Climatol., 104(3–4), 301–312,
763 doi:10.1007/s00704-010-0341-4, 2011.
764 Zhuang, B. L., Li, S., Wang, T. J., Deng, J. J., Xie, M., Yin, C. Q., and Zhu, J. L.: Direct radiative
765 forcing and climate effects of anthropogenic aerosols with different mixing states over China,
766 Atmos. Environ., 79, 349–361, doi:10.1016/j.atmosenv.2013.07.004, 2013b.

767 Zhuang, B. L., Liu, Q., Wang, T. J., Yin, C. Q., Li, S., Xie, M., Jiang, F., and Mao, H. T.: Investigation
768 on semi-direct and indirect climate effects of fossil fuel black carbon aerosol over China, Theor.
769 Appl. Climatol., 114, 651–672, doi:10.1007/s00704-013-0862-8, 2013a.
770 Zhuang, B. L., Wang, T. J., Li, S., Liu, J., Talbot, R., Mao, H. T., Yang, X. Q., Fu, C. B., Yin, C. Q.,
771 Zhu, J. L., Che, H. Z., and Zhang, X. Y.: Optical properties and radiative forcing of urban aerosols
772 in Nanjing, China, Atmos. Environ., 83, 43–52, 2014a.
773 Zhuang, B. L., Wang, T. J., Liu, J., Li, S., Xie, M., Yang, X. Q., Fu, C. B., Sun, J. N., Yin, C. Q., Liao, J.
774 B., Zhu, J. L., and Zhang, Y.: Continuous measurement of black carbon aerosol in urban Nanjing of
775 Yangtze River Delta, China, Atmos. Environ., 89, 415–424, 2014b.
776 Zhuang, B. L., Wang, T. J., Liu, J., Ma, Y., Yin, C. Q., Li, S., Xie, M., Han, Y., Zhu, J. L., Yang, X. Q.,
777 and Fu, C. B.: Absorption coefficient of urban aerosol in Nanjing, west Yangtze River Delta, China,
778 Atmos. Chem. Phys., 15, 13633–13646, 2015.

779 **Figure captions:**

780 Figure 1. The 10th, 25th, median, 75th, and 90th percentiles of 550 nm AAC (a, Mm^{-1}), 470/660 nm
781 AAE (b), 550 nm SC (c, Mm^{-1}), 550 nm (d, Mm^{-1}) and 450/635 nm SAE (e) in each season from March
782 2014 to Feburay 2016.

783 Figure 2. Seasonal means (markers) and corresponding standard deviations (error bars) of
784 wavelength-dependent AAC (a, Mm^{-1}), SC (b, solid mark, Mm^{-1}), Bsp (b, open mark, Mm^{-1}), EC (c,
785 Mm^{-1}), SSA (e) and ASP (f) at 450, 532, 550, 635 nm, as well as AAE at 470/660 nm (d, red solid mark)
786 and SAE at 450/635 nm (d, green open mark)

787 Figure 3. Diurnal variations of 550 nm AAC (a, Mm^{-1}), SC (b, Mm^{-1}), Bsp (c, Mm^{-1}), SSA (d), ASP (g),
788 470/660 nm AAE (e) and 450/635 nm SAE (f) during the study period.

789 Figure 4. Frequency (%) distributions of 550 nm AAC (a), SC (b), Bsp (c), SSA (d), ASP (g), 470/660
790 nm AAE (e) and 450/635 nm SAE (f) on annual (shaded bar) and seasonal (markers in colors) scales.
791 Figure 5. Clusters of 96-h back trajectories arriving at the study site at 100 m in JJA (a) and DJF (b)
792 simulated by the HYSPIT model. The means with standard deviations of the aerosol optical properties
793 at each cluster of back trajectories in both JJA and DJF are plotted in Fig. 5c and 5d, respectively.
794 Figure 6. Relationships between 550 nm AAC and SC (solids square in blue) and between 550 nm Bsp
795 and SC (solid cycles in gray) in spring (a), summer (b), autumn (c) and winter (d).
796 Figure 7. Relationships between the 550 nm ASP and SC in different RH levels.
797 Figure 8. Relationships between the monthly mean values of 491 nm SSA and extinction Angstrom
798 exponent (EAE) at 491/863 nm (a) and between the monthly mean values of SSA difference (863-491
799 nm) and EAE at 491/863 nm (b).
800 Figure 9. Seasonal variations of RH (a, %) and linear correlations between AAE and RH (b, light blue,
801 upper), between SAE and RH (b, green, middle), and between ASP and RH (c, deep blue, lower).
802 Figure 10. Relationships between SC and visibility (open cycles) and between EC and visibility (solid
803 cycles) in different RH levels in spring (a), summer (b), autumn (c) and winter (d).
804 Figure 11. Relationships between SSA and visibility (solid cycles) and between ASP and visibility
805 (solid squares) in different RH and AAE levels in spring (a), summer (b), autumn (c) and winter (d).
806 Figure 12. Relationships between surface EC at 550 nm and column AOD at 500 nm in spring (a),
807 summer (b), autumn (c) and winter (d).
808
809 **Table captions:**
810 Table 1 Statistical summary of the surface aerosol optical properties in Nanjing.

811 Table 2 Seasonal mean±SD of the surface aerosol optical properties in Nanjing.

812 Table 3. The dominant and maximum frequencies as well as corresponding ranges of the aerosol

813 optical properties.

814 Table 4 The aerosol optical properties in Nanjing and at other sites of China.

815

816

817 Table 1 Statistical summary of the surface aerosol optical properties in Nanjing

Factors	Max	Min	Mean±SD	Median
550 nm AAC (Mm^{-1})	230.648	1.439	29.615±20.454	24.572
550 nm SC (Mm^{-1})	2493.092	20.673	338.275±228.078	284.379
550 nm Bsp (Mm^{-1})	300.101	1.401	44.257±27.396	38.206
550 nm EC (Mm^{-1})	2643.101	31.186	381.958±252.271	321.679
550 nm SSA	0.988	0.404	0.901±0.049	0.908
550 nm ASP	0.908	0.118	0.571±0.088	0.582
470/660 nm AAE	3.256	0.145	1.583±0.228	1.592
450/635 nm SAE	3.344	0.162	1.320±0.407	1.317

818 AAC: Aerosol absorption coefficient

819 SC: Aerosol scattering coefficient

820 Bsp: Aerosol back scattering coefficient

821 SSA: Aerosol single scattering albedo

822 ASP: Aerosol asymmetry parameter

823 AAE: Ångström exponent of absorbing aerosols

824 SAE: Ångström exponent of scattering aerosols

825

826 Table 2 Seasonal mean±SD of the surface aerosol optical properties in Nanjing

Factors	MAM	JJA	SON	DJF
550 nm AAC (Mm^{-1})	26.954±18.632	19.653±15.689	33.474±19.686	37.958±21.892
550 nm SC (Mm^{-1})	318.998±202.264	340.865±226.151	294.624±200.052	385.137±255.282
550 nm Bsp (Mm^{-1})	42.995±23.580	36.990±25.067	38.684±23.017	54.786±30.974
550 nm EC (Mm^{-1})	341.279±209.315	370.236±248.125	351.887±244.267	422.569±273.565
550 nm SSA	0.915±0.043	0.933±0.049	0.874±0.053	0.890±0.040
550 nm ASP	0.553±0.086	0.638±0.069	0.566±0.079	0.540±0.083

470/660 nm AAE	1.571±0.172	1.488±0.263	1.524±0.277	1.701±0.156
450/635 nm SAE	1.097±0.320	1.337±0.428	1.544±0.352	1.235±0.383

827

828 Table 3. The dominant and maximum frequencies as well as corresponding ranges of the aerosol
829 optical properties.

The aerosol optical properties	The dominant Bins	The dominant Frequencies	The maximum Bins	The maximum Frquencies
AAC	9~45 Mm^{-1}	73%	9~21 Mm^{-1}	32.9%
SC	60~390 Mm^{-1}	67%	170~280 Mm^{-1}	24.04%
Bsp	15~60 Mm^{-1}	69%	30~45 Mm^{-1}	26.45%
SSA	0.87~0.97	73%	0.91~0.93	18.64%
AAE	1.4~1.8	71%	1.5~1.6	20.9%
SAE	0.96~1.68	62%	1.32~1.5	18.06%
ASP	0.48~0.69	81%	0.55~0.62	34%

830

831 Table 4 The aerosol optical properties both in Nanjing and at other sites of China

Site	Period	AAC (Mm^{-1})	SC (Mm^{-1})	ASP	SSA	Method	References
Nanjing (urban)	2014.3-2016.2	29.6 (550 nm)	338.3 (550 nm)	0.57 (550 nm)	0.9 (550 nm)	[a] AE-31 [b] Aurora 3000	This stuty
Beijing (urban)	2005-2006	56 (532 nm)	288 (525 nm)	/	0.8 (525 nm)	[c] AE-16 [d] M9003	He et al. (2009)
Beijing (rural)	2003-2005	17.5 (525 nm)	174.6 (525 nm)	/	0.88 (525 nm)	[a] AE-31 [d] M9003	Yan et al. (2008)
Xi'an (urban)	2009	/	525 (520 nm)	/	/	[e] Auroral 1000	Cao et al. (2012)
Chengdu (urban)	2011	96 (532 nm)	456 (520 nm)		0.82	[a] AE-31 [f] Aurora 1000G	Tao et al. (2014)
Wuhan (urban)	2009.12-2014.03	119 (520 nm)	377 (550 nm)	/	0.73 (520 nm)	[a] AE-31 [g] Model 3563	Gong et al. (2015)
Xinken (rural)	2004.10-2011.05	70 (550 nm)	333 (550 nm)	/	0.83 (550 nm)	[h] MAAP [g] Model 3563	Cheng et al. (2008)
Tongyu (rural)	Spring, 2010 Spring, 2011	7.61 (520 nm) 7.01 (520 nm)	89.2 (520 nm) 85.3 (520 nm)	/ /	0.9 (520 nm)	[a] AE-31 [b] Aurora 3000	Wu et al. (2012)
Nanjing (suburban)	2011.03-04	28.1 (532 nm)	329.3 (550 nm)	/	0.89 (532 nm)	[i] PASS [d] Model 3563	Yu et al. (2016)
Shanghai (ruban)	2010.12-2011.03	66 (532 nm)	293 (532 nm)	/	0.81 (532 nm)	[a] AE-31 [g] Model 3563	Xu et al. (2012)
Shouxian (rural)	2008.5-12	29 (550 nm)	401 (550 nm)	/	0.92 (550 nm)	[j] Model PSAP [g] Model 3563	Fan et al. (2010)
Lanzhou (urban)	Winter 2001, 2002	/	226 (550 nm)	/	/	[d] Model 3563	Zhang et al. (2004)
Panyu (urban)	Spring and winter, 2008	84.03 and 188.8 (532 nm)	/	/	/	[a] AE-31	Wu et al. (2013)
Dongguan (suburban)	Spring and winter, 2008	47.1 and 95.53 (532 nm)	/	/	/	[a] AE-31	Wu et al. (2013)

Maofengshan (Rural)	Spring and winter, 2008	26.45 and 28.77 (532 nm)	/	/	/	[a] AE-31	Wu et al. (2013)
Yongxing Island	Spring and winter, 2008	7.21 and 8.37 (532 nm)	/	/	/	[a]AE-31	Wu et al. (2013)

[a] Seven channels Aethalomter (model AE-31, Magee Scientific, USA)

[b] Three wavelength integrating Nephelometer (Model Aurora 3000, Australia)

[c] Aethalometer AE16

[d] Nephelometer M9003

[e] Integrating Nephelometer (Model Aurora 1000)

[f] Integrating Nephelometer (Model Aurora 1000G)

[g] Integrating Nephelometer (Model 3563, TSI, USA)

[h] Multi-angle Absorption Photometer (MAAP, Thermo, Inc., Waltham, MA USA, Model 5012)

[i] Photo acoustic Soot Spectrometer (PASS 1, DMT, USA)

[j] Particle/SootAbsorption Photometer

Figures:

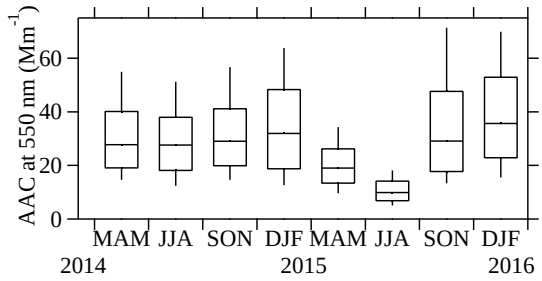

a)

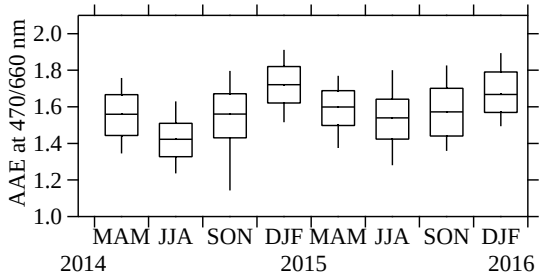

b)

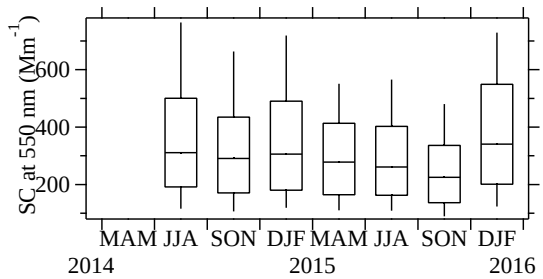

c)

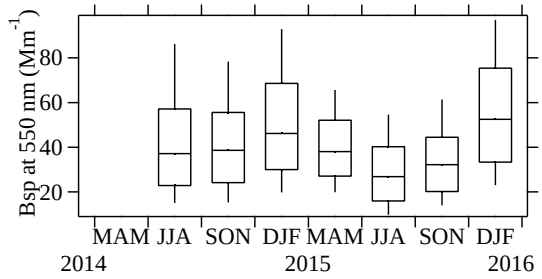

d)

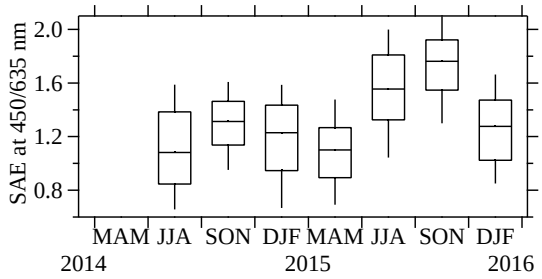

e)

Figure 1.

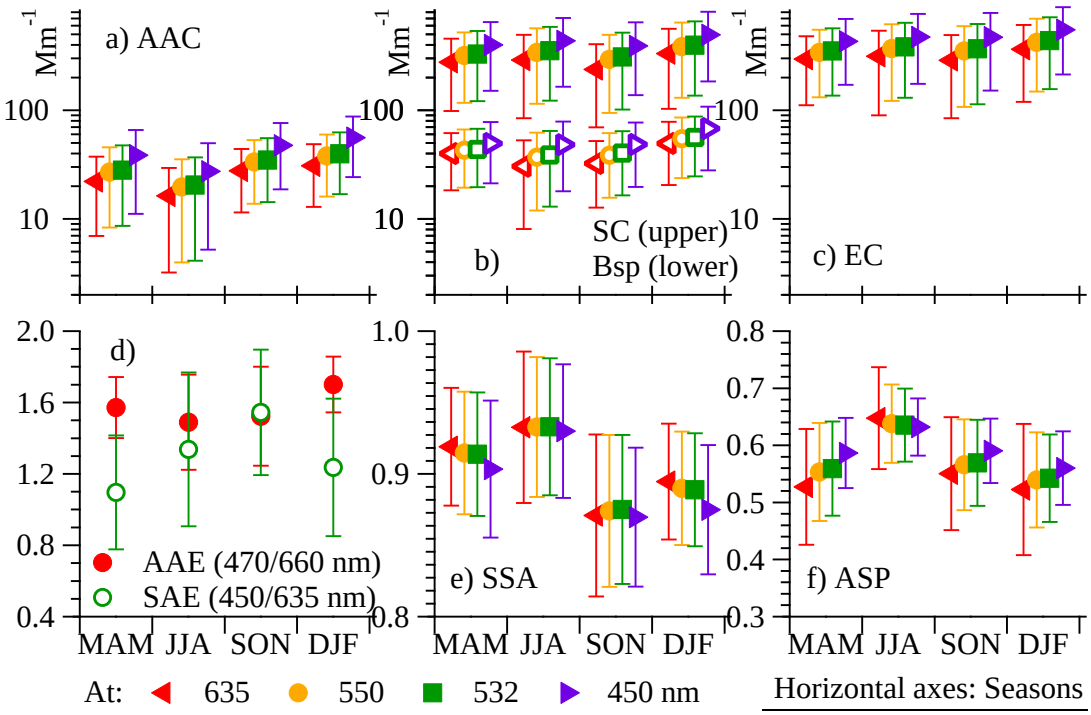

Figure 2.

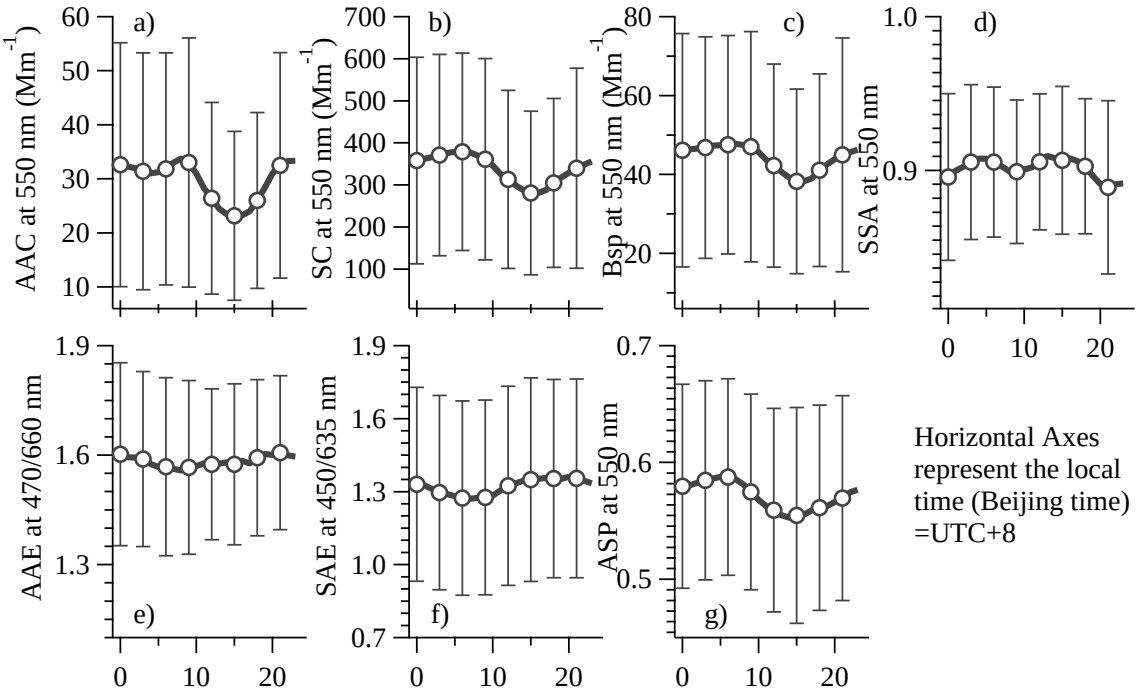

Figure 3

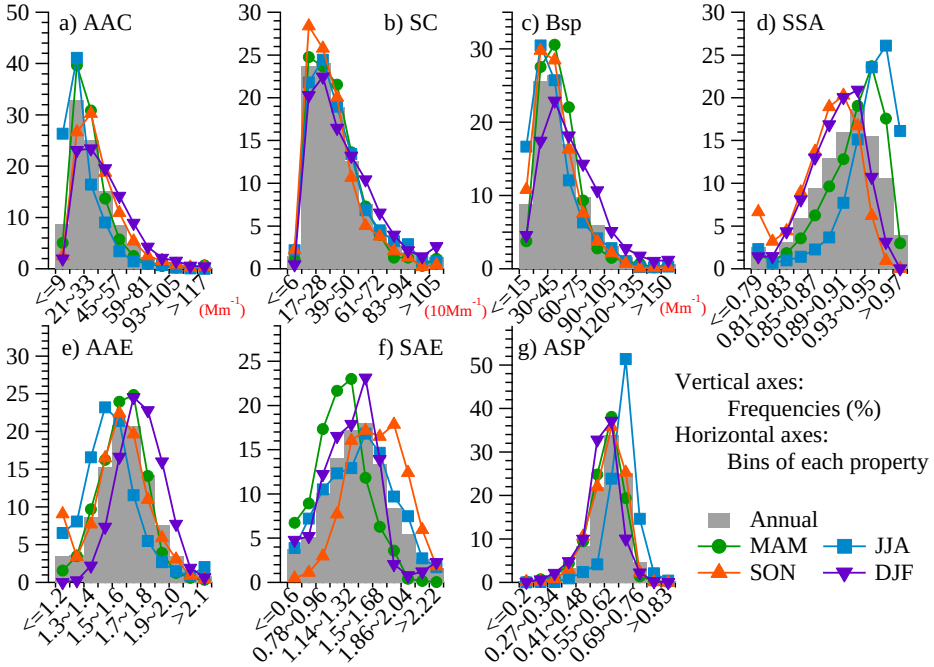

Figure 4

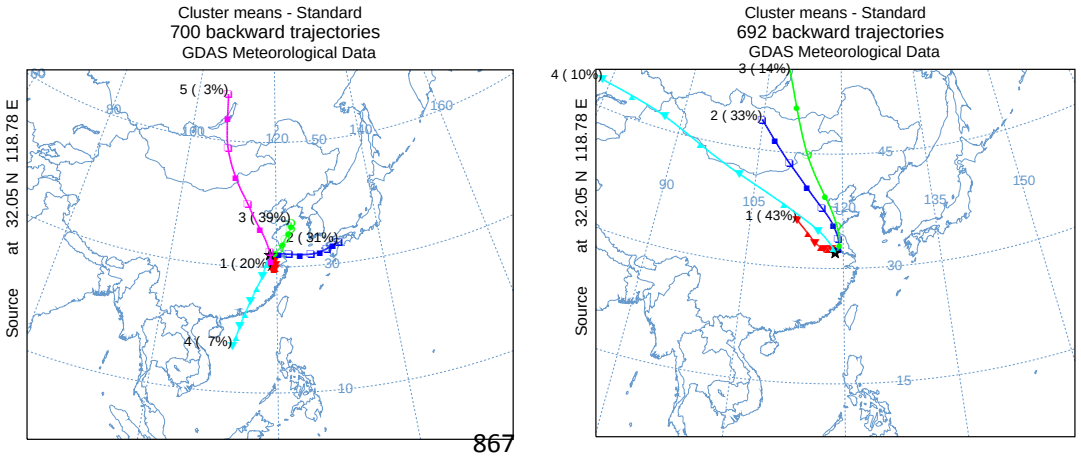

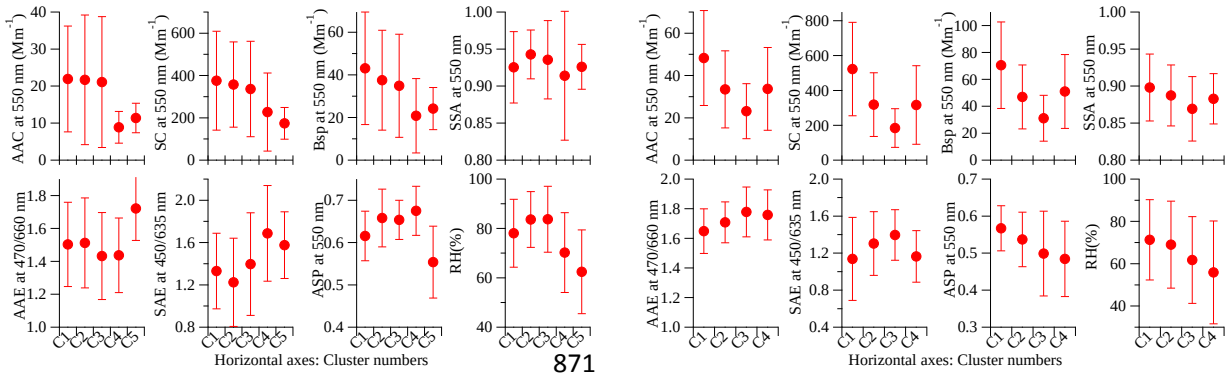

Figure 5

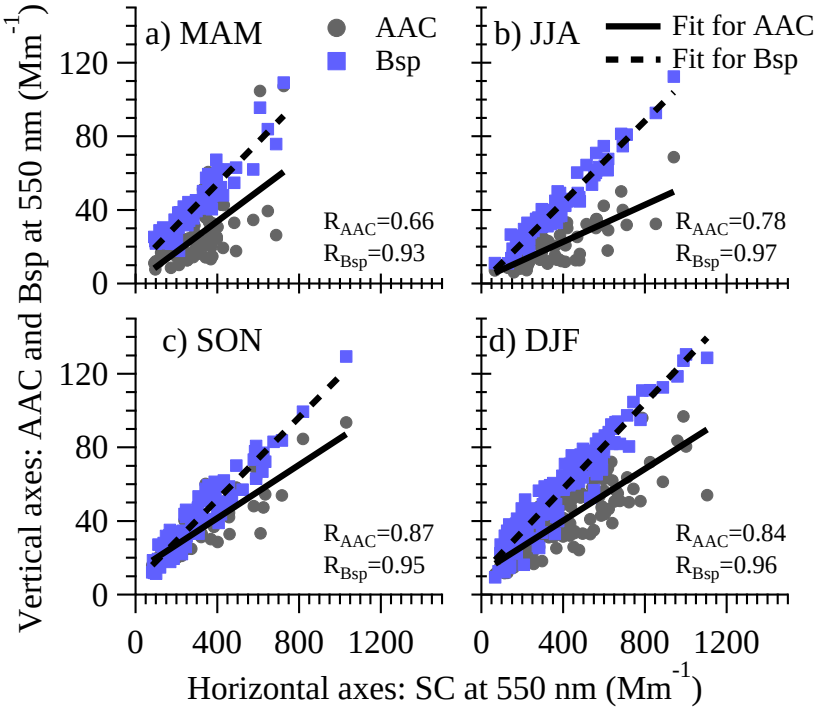

Figure 6

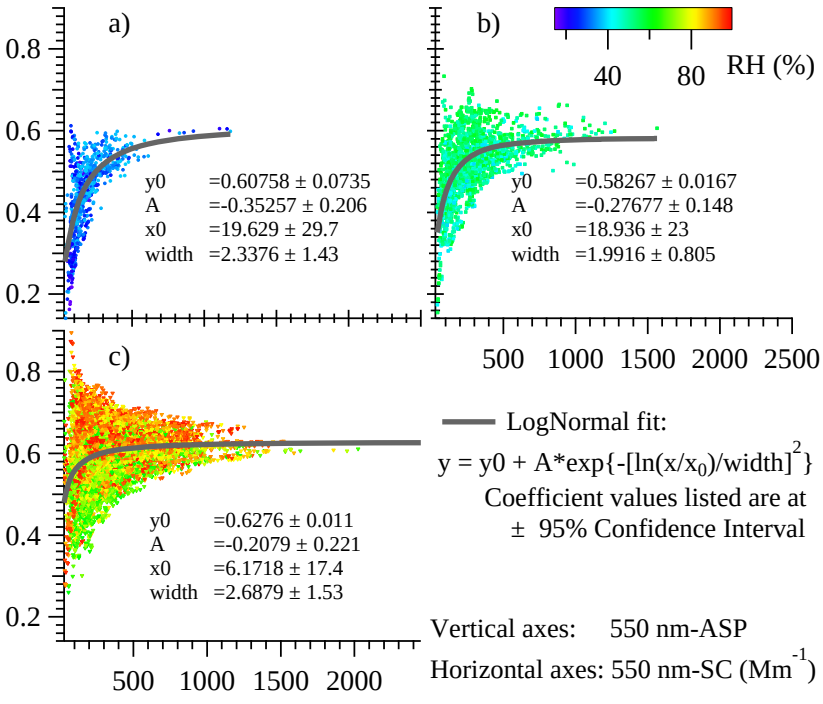

Figure 7

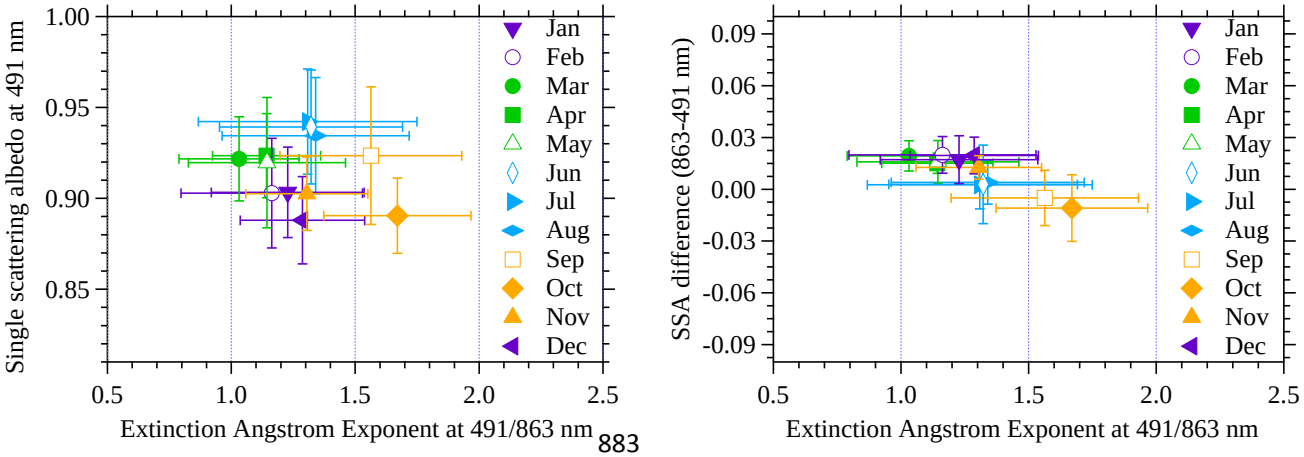

a) b)

Figure 8

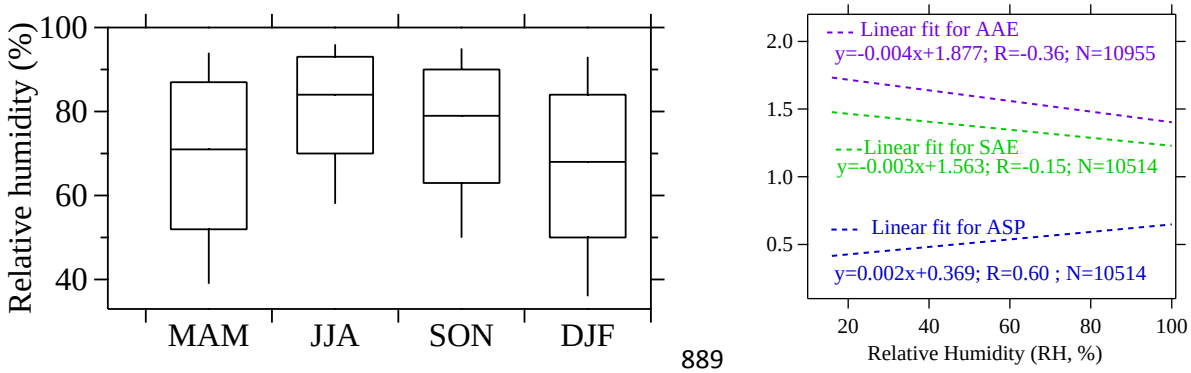

a) b)

Figure 9

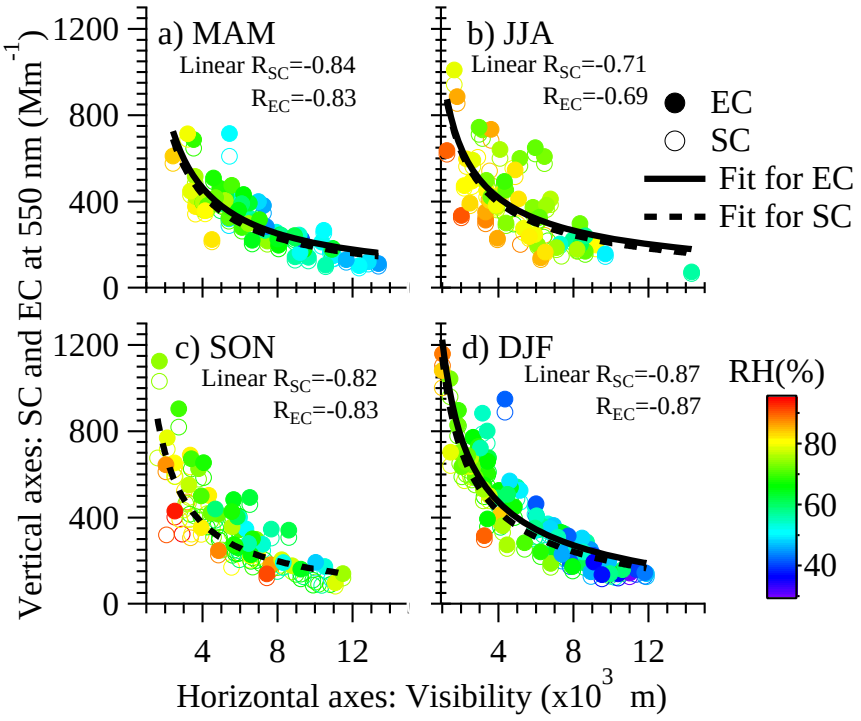

892

893 Figure 10

894

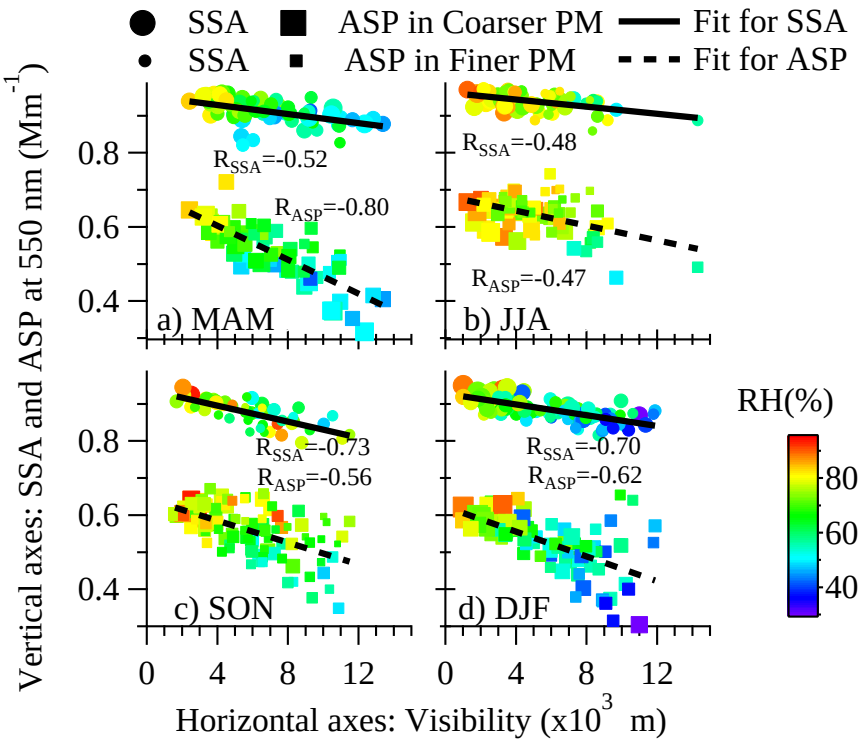

895

896 Figure 11

897

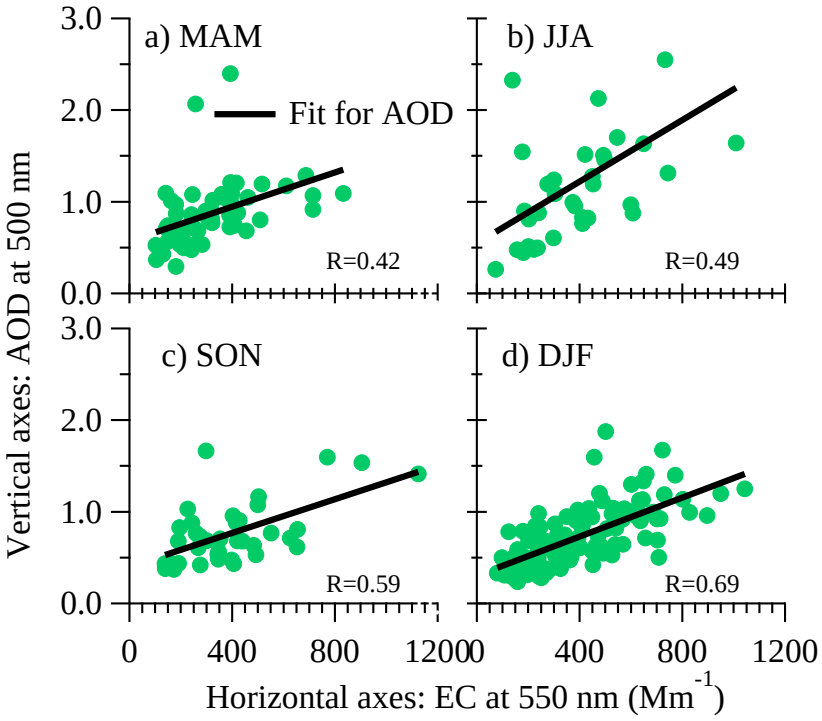

898

899 Figure 12